Deterministic seismic hazard assessments through hybrid ground motion simulation

Case studies for Wenchuan, China and İzmir, Turkey

Louise Wedderkopp Bjerrum

Dissertation for the degree philosophiae doctor (PhD)
at the University of Bergen

June 2011

Preface

The work presented in this thesis was initiated in August 2007 when I was admitted to the PhD program at the University of Bergen (UiB). The thesis is divided into two parts. The first part is a summary of my work done during my time as a PhD candidate at the Department of Earth Science. Also, some background and future perspectives for the study are included in the summary. The second part consists of a collection of five research papers, all of which are either published or in review in international journals and conference proceedings. This is the main outcome of my studies.

The thesis concerns deterministic seismic hazard assessment using a broadband frequency ground motion simulation technique. I have worked with two different tectonic settings and problems, and the research papers can be divided into two groups. The first group concerns a retrospect study of the 2008 M_w 7.9 Wenchuan, China earthquake, where ground motion simulations are calculated and different possible slip distributions across the fault plane are discussed. The work serves as a verification study of the applied simulation method. A visit to the earthquake affected area in October 2008, partly sponsored by the "Norwegian Society for Earthquake Engineering" (Norsk Jordskjelvteknisk Forening) served as the basis for comparing the simulated ground motions with the observed damage for various sites along the fault zone. The second group of papers deals with hazard assessment for İzmir, Turkey and the surrounding area. The area has not experienced significant earthquakes in more than 230 years. Therefore, this part serves as a predictive study. The most significant faults in terms of seismic hazard in İzmir are first identified. Following, the variation in the simulation results due to uncertainties in the input parameters is identified. Finally, site effect potential for various locations within İzmir is considered, and estimates of ground motion taking soil conditions into account are presented. The last part was based on field work in İzmir, and was financially supported by "The Meltzer Fund" (L. Meltzers Høyskolefond).

Louise Wedderkopp Bjerrum,
April 2011

Acknowledgements

I am grateful to a large number of people who have supported me during my PhD on a professional and a personal level.

First I would like to thank my supervisors Kuvvet Atakan, Lars Ottemöller and Mathilde Sørensen for supervision, support and many fruitful discussions during my studies. I would like to thank Coskun Sari for valuable support during fieldwork, and for always making my stays in İzmir memorable. Also, I am very appreciative for the help during fieldwork provided by several PhD students at Dokuz Eylül University in İzmir, Turkey. I would like to thank Matthias Orhnberger for useful and interesting discussions on my research. Additionally, I would like to thank Harald Walderhaug, Henk Keers, Olav Eldholm, Atle Austergaard, Mohammad Raeesi, Norbjørg Kaland, Inger Karlsen Trine Lise Stjernholm and Hanne Israelsen from the Department of Earth Science for discussions, support and help to solve many practical issues.

I am thankful to the Department of Earth Science, University of Bergen which has provided the financial support for my PhD studies. Also, I have received grants for fieldworks from both the Norwegian Society for Earthquake Engineering and from the Meltzer Fund for which I am very grateful.

The present thesis has greatly benefitted from comments and suggestions from my supervisors, Harald Walderhaug, Henk Keers, Erling Hugo Jensen and Katarina Gobo. Mo Yan Yuen has done an enormous work correcting language, only for the salary of hot chocolate and French cheeses.

I have been blessed with great student assistants in the introduction geophysics course on which I have been teaching during my time at the Department of Earth Science. I would like to thank Elin Vormestrand Andreassen, Brikt Apeland, Anita Hovet, Stine Tjomlid Maal, Ingrid Vold and Iselin Aarseth for their support. Also, I am grateful to Trond Kvarven for taking over in the last part of the semester in spring 2011.

I wish to thank my friends in Denmark and Norway. I am grateful to the friends “at home” for always taking their time to see me in my sometimes rather hectic plans and with very short notice, during my stays in Denmark. Especially I would like to mention Anne Katrine Alsing, Ditte Maria Grønhøj, Stine Kildegaard Poulsen and Kathrine Dam Andersen. During the six and a half years in Norway I have met many great people. First of all, I want to mention Mo Yan Yuen and Øystein Alsaker. Their great humour and good taste in coffee, wine and food have contributed to many joyful memories. I want to thank the *board gamers/lunch eaters* (Vaneeda Allken, Edward-Benedict Brodie, Zoltán Erdõs, Katarina Gobo, Suzon Jammes and Erling Hugo Jensen) for many ecstatic and enthusiastic gaming sessions and many crazy and weird discussion topics during lunch hours. Last but not least I want to thank Torunn Lutro and Åse Oliv Bjørge - field work without you would not have been as fun!

At the end I want to thank my family. My parents - mom, “step-mom”, dad and step-dad - Alice Wedderkopp, Anette Hald-Bjerrum, Jakob Bjerrum and Ole Frandsen, who have been a tremendous support in my considerations and decision of continuously extending my stay in Bergen and always making sure I had a place to come home to. Also, the moral support during the last hectic months while finishing my thesis is appreciated. I wish to thank my cousin Mette Bjerrum Koch, with whom I always have many fun hours with, either in Bergen or in Copenhagen. She has been an enormous support when everything seems to fall apart! Finally, I am grateful for the support from Jimmy Paillet, who has been keeping me company late at night while I have been writing.

Abstract

In areas with potential for large earthquakes, ground motion simulation based on earthquake rupture scenarios serve as an important tool to quantify the seismic hazard in terms of expected ground shaking. A kinematic hybrid broadband frequency simulation technique, combining deterministic low frequency modeling with stochastic high frequency modeling, is applied in a retrospect and a predictive study in order to assess the seismic hazard. The geographical focus in this thesis is on the region of the M_w 7.9 2008 Wenchuan, China earthquake and the city of İzmir, Turkey.

On 12 May 2008, a devastating earthquake of M_w 7.9 occurred in the Sichuan Province of China. The earthquake had disastrous consequences and took more than 80,000 lives. The rupture occurred along a 300 km long fault dipping northwest along the Longmen Shan fold-thrust belt, which separates the Tibetan Plateau in the northwest from the Sichuan Basin in the southeast. The earthquake is simulated using three available finite-fault slip models as input in the earthquake rupture scenarios. Acceleration values of the order of 1 g are simulated, which is close to what was recorded during the event. The simulation results reveal large variations in ground shaking due to the rupture complexity in terms of a variety of factors, including the location of asperities and the width of the fault plane. However, the simulated and observed ground motions are comparable in terms of ground shaking level and frequency content. Furthermore, from a field reconnaissance trip in October 2008, it is evident that extensive damage occurred over a wide area due to the shear size of the earthquake rupture combined with poor building practices. The combination of several factors, including mountainous landscape, strong ground shaking, extensive landslides and rock-falls, has exacerbated the human and economic consequences of this earthquake.

West-ward migration and counter-clockwise rotation of the Anatolian microplate in the Aegean Sea result in reactivation of several faults along the west coast of Turkey, which produce destructive earthquakes. İzmir, the third largest city in Turkey, has been destroyed by earthquakes several times in recent history, latest

in 1778 and the seismic hazard for the city is assessed in three parts. The first part concerns identification of the faults that control the seismic hazard in the area. Nine different earthquake rupture scenarios along recognized faults in the area are defined, based on existing knowledge of source parameters from earthquakes in similar tectonic regimes. From the ground motion simulations the largest peak ground motions in İzmir are associated with two faults, the İzmir fault (normal) which lies underneath the city and the Tuzla fault (strike-slip) which lies southwest of the city.

The level and distribution of simulated ground shaking from ground motion simulation studies based on earthquake rupture scenarios is highly dependent on the input parameters used in the calculations. The second part of the hazard assessment for İzmir concerns the variability of the simulated ground motions, due to uncertainties in the input parameters. In this part the uncertainties of the input parameters are considered by calculating ground motions for a number of scenarios, while varying the input parameters. The level of ground motion is found to be most sensitive to the velocity model, seismic moment, rise time and rupture velocity. Stress-drop and attenuation control the change in ground motion levels to a large extent, if they are changed sufficiently. Low frequency ground motion is mostly affected by the location of rupture initiation, seismic moment, fault depth, rise time and crustal velocity model. The largest variability in the simulated ground motion is found close to the fault plane, coinciding with the center of İzmir. The standard deviation of all the simulations exceeds 200 cm/s^2 and 20 cm/s for peak ground acceleration and peak ground velocity, respectively.

İzmir, being located on thick sedimentary deposits, is vulnerable to local site effects during strong ground shaking and it is therefore important to consider these when assessing the seismic hazard. In the last part of this study, local site effects are considered by evaluating transfer functions obtained from H/V spectral ratios of ambient noise. The ground motion, taking into account the soil layer, is then calculated as a convolution of the simulated waveform with the transfer function. Additionally, for the Karşıyaka district in İzmir, a soil column is modeled by theoretically calculating the soil response and comparing this to the obtained H/V spectral ratios. Considering the soil layer in the calculated ground motions suggests an increase in ground shaking due to the soil response. Furthermore, potential of soil deformation, such as liquefaction, during an earthquake is expected for the northern and innermost parts of İzmir Bay. Larger amplification of the seismic waves is calculated for a thicker soil column.

Although assessing the seismic hazard through ground motion simulations gives valuable information, such as expected ground shaking level and frequency content of the seismic waves, it is important to keep in mind that the question of probability of occurrence of the simulated earthquake is not considered in such a seismic hazard assessment. The applied methodology successfully reproduces the strong ground motion distribution and frequency content of seismic waves in retrospect studies and the simulation method is found appropriate in order to obtain realistic ground motion estimates for predictive studies. The importance of considering several possible rupture scenarios along the same fault when assessing the deterministic seismic hazard is shown, since uncertainties in the input parameters result in large variability of the simulated ground motion.

List of papers

Paper 1: Bjerrum, L.W., Sørensen, M.B. and Atakan, K. (2010). Strong ground-motion simulation of the 12 May 2008 M_w 7.9 Wenchuan earthquake, using various slip models. Bulletin of the Seismological Society of America, Vol. 100, No. 5B, pp. 2396–2424, November 2010, doi: 10.1785/0120090239.

Paper 2: Bjerrum, L.W., Atakan, K. and Sørensen, M.B. (2010). Reconnaissance report and preliminary ground motion simulation of the 12 May 2008 Wenchuan earthquake. Bulletin of Earthquake Engineering, Vol. 8, No. 6, pp. 1569–1601, December 2001, doi: 10.1007/s10518-010-9198-2.

Paper 3: Bjerrum, L.W. and Atakan, K. (2008). Scenario based ground motion simulations for assessing the seismic hazard in İzmir, Turkey. Proceedings of the 14th World Conference on Earthquake Engineering, Beijing, China, 12-17 October 2008.

Paper 4: Bjerrum, L.W. Sørensen, M.B., Ottemöller, L. and Atakan, K. (*in review*). Sensitivity of simulated ground motions due to input parameter uncertainty: Case study for İzmir, Turkey. *Submitted* to Bulletin of the Seismological Society of America.

Paper 5: Bjerrum, L.W., Lutro, T., Sørensen, M.B., Ottemöller, L., Sari, C. and Atakan, K. (*in review*). Simulated ground motions with site effect potential evaluated through transfer functions and H/V measurements: Case study for İzmir, Turkey. *Submitted* to Bulletin of Earthquake Engineering.

Contribution and motivation to the individual papers

The work on Paper 1 ("Strong ground-motion simulation of the 12 May 2008 M_w 7.9 Wenchuan Earthquake, using various slip models") was initiated following the May 12, 2008 Wenchuan earthquake. Preliminary results were presented in the special session on the earthquake during the 14th World Conference on Earthquake Engineering. The motivation of the study was a retrospect verification study focusing on the performance of the ground motion simulation technique to reproduce the experienced ground motions. As several slip models became available and the complexity of the rupture became apparent, discussions on fault width and focal mechanism were raised, and the study changed focus to also include possible evaluation of the published slip models based on the simulation results. The first version of the ground motion simulations were conducted already in June 2008. They were finalized in spring 2009 after several improvements of the input models. I estimate my contribution to the paper to be 85%.

The study of Paper 2 ("Reconnaissance report and preliminary ground motion simulation of the 12 May 2008 Wenchuan earthquake") was motivated by a visit, October 17-18 2008, to the area affected by the May 12, 2008 Wenchuan earthquake. The trip was a post conference trip of the 14th World Conference on Earthquake Engineering, and was co-sponsored and organized by the Earthquake Administration of Sichuan Province, Sichuan Provincial Department of Construction and Sichuan Association for Science & Technology. I wanted to present the observed damage to structures and compare these with a simulation of the ground motions for the earthquake. The simulation presented in this paper is from the preliminary work on the simulation of the earthquake initiated for the study in Paper 1. However, the simulation results presented in the two papers are not identical due to further improvements of the input models used in Paper 1. I estimate my contribution to Paper 2 to be 80%.

Paper 3 ("Scenario based ground motion simulations for assessing the seismic hazard in İzmir, Turkey") was initiated during my work for my master thesis

from May 2007. This study was motivated by the fact that İzmir, the third largest city in Turkey, is located close to several active faults, which have ruptured several times throughout history. Therefore, an important issue, when it comes to seismic hazard in İzmir, is the identification of the faults posing the largest threat. The input models for the earthquake scenarios were improved from my master thesis during the work with the preparation of the manuscript of this paper. I estimate my contribution to the paper to be 80%.

The study presented in Paper 4 ("Sensitivity of simulated ground motions due to input parameter uncertainty: Case study for İzmir, Turkey") was based on the identification of the İzmir fault to pose the largest seismic threat to the city of İzmir in Paper 3. The input parameters used in the ground motion simulations in Paper 3 are based on literature of recent earthquakes in similar tectonic settings, and the ground motion simulations are affected by uncertainties in the input parameters. This study aims to quantify the expected uncertainties in predictive ground motion simulation studies. This study was initiated in 2008. However, the simulations were first finalized in autumn 2010 due to the shift in the focus by the studies concerning the Wenchuan earthquake. I estimate my contribution to the paper to be 90%.

In Paper 5 ("Simulated ground motions with site effect potential evaluated through transfer functions and H/V measurements: Case study for İzmir, Turkey") the site effect potential in İzmir, which is located on large sediment deposits, is considered. In the simulations presented in Paper 3 and 4, ground motions were calculated for bedrock conditions. In this study we use H/V spectral ratios of ambient noise as estimates of transfer functions to obtain ground motions for soil conditions of selected sites within İzmir. In addition, estimates of simple soil structures are modeled on the base of theoretically calculated soil response, which are compared to the H/V spectral ratios. The microtremor data used for the H/V spectral ratio analysis was collected during a 15-day field work in İzmir in March-April 2010. The field work was done in collaboration with Coskun Sari, Department of Geophysics, Dokuz Eylül University, İzmir, Turkey. Torunn Lutro, University of Bergen, performed the processing of the microtremor data and the modeling of the soil structures. My main contribution to the paper is in ground motion simulation, data collection, analysis and evaluation of transfer functions from the H/V spectral ratios, computations of the soil ground motion and in the writing process. I estimate my contribution to the paper to be 70%.

Table of Contents

1

Part I: Summary

1. Introduction

In areas of potential large earthquakes, seismic hazard assessment is an important tool to quantify the ground shaking which can be expected. Seismic hazard assessment can be done probabilistically, deterministically or by a combination of the two. The probabilistic analysis determines the probability of exceeding a specific ground motion level within a certain time period. This analysis is based on earthquake catalogs, recurrence relationships and ground motion attenuation relations. This approach therefore considers previous seismicity of an area, and takes several possible earthquake sources into account. The earthquake recurrence is either time-independent (Poissonian) or has a time dependency. In the time-independent assumption an earthquake source is expected to have no memory, and earthquakes can occur anywhere within a given source zone at any time. In the time-dependent models, the probability of future earthquake occurrence depends on the time passed since the latest large earthquake (Reiter, 1990). In the deterministic approach, the focus is on a single earthquake scenario with no information of the rupture probability available. The effect of an earthquake at a given site is evaluated by empirical seismic attenuation relations or by simulating the earthquake rupture scenario. From such simulations, information of the expected frequency content and ground shaking level can be retrieved. The work presented in this thesis concerns ground motion simulations, using a hybrid broadband simulation technique. The objective of the study is to assess the seismic hazard in two regions with a high level of seismic activity.

1.1 Overview of ground motion simulation techniques

Deterministic seismic hazard assessed through ground motion simulations is either based on kinematic or dynamic approaches. In the kinematic approaches, parameters such as the slip distribution and faulting area are given as input. In the dynamic approaches, on the other hand, the earthquake is studied using stresses and friction laws (e.g. Archuleta and Day, 1980; Archuleta and Fraizer,

1978; Madariaga, 1976). In the following paragraphs some of the existing simulation techniques are summarized. The main focus is on the kinematic approaches, as this is the technique used in this thesis.

Kinematic ground motion simulation

Kinematic ground motion simulation methods can be divided into three main groups: deterministic wave propagation (low frequencies), stochastic (high frequencies) and hybrid (broad band) (Hartzell et al., 1999). In the deterministic wave propagation a kinematic source model is defined and the slip along the fault must be known. This method can simulate ground motions for the lower frequencies. In the stochastic approach, earthquake ground motion is modeled as random noise for higher frequencies and the spectral shape is given by the ω^2-model (Beresnev and Atkinson, 1997; 1998; Boore, 2003; Brune, 1970). Hybrid methods are a combination of the wave propagation and stochastic methods for the two frequency ranges (e.g. Hartzell et al., 2005; Liu et al., 2006; Somerville et al., 1991).

In both the wave propagation for lower frequencies and in stochastic models for the higher frequencies, simulations of the Empirical Green's Function (EGF) method (Hartzell, 1978) is one of the most commonly used techniques. The simulation of the earthquake is done by subdividing the fault plane into a distribution of point sources. The EGF is taken as the response of the point sources from recordings of the aftershocks closest to the point source. Finally, summing all the contributions, while taking the phase delay into account, gives the simulated ground motion of the main event. With the EGF method the combined effect of the source process and wave propagation is considered in a simple procedure. This cannot be predicted with simplified 1D or purely stochastic methods. Using EGF requires recording of small events from the area of the event to be simulated, which can be applied as Green's functions. This can be a disadvantage, since such recordings are rare, especially for areas prone to large infrequent earthquakes (Kamae et al., 1998). For retrospect studies of large earthquakes, recorded aftershocks can be used as Green's functions in the calculations of the ground motions caused by the main event. However, the aftershocks adopted as EGF must be well distributed along the fault plane and have the same focal mechanism as the main shock. Furthermore, each aftershock must be recorded at the same stations as the main event. In this simulation approach it is important to adopt aftershocks of a magnitude large enough to

excite response in the earth. However, it is also important that the magnitude of the aftershock is small enough to be regarded a point source (Hartzell, 1978).

Recordings of small earthquakes or aftershocks on a specific fault are not always available. For such cases the Hybrid Green's Function (HGF) technique, which computes synthetic Green's functions, was developed (Pitarka et al., 2000; Somerville et al., 1991). The Green's functions are calculated using a hybrid technique by combining two different methods: one used to calculate the low-frequency ground motion, the other to compute the high-frequency ground motion (Kamae et al., 1998; Hartzell et al., 1999; Pitarka et al., 2000). In the HGF technique, the high-frequency ground motion is computed using a stochastic method with a high-frequency cut-off frequency and a frequency dependent Q-value following Boore (1983). The low-frequency ground motion is obtained by assuming a point source model and adopting a crustal velocity structure (1D or 3D). The HGF are computed as a combination of the low- and high-frequency ground motions. The strong ground motion from the large earthquake is obtained from summation of the HGF, using the same technique as for the EGF (Kamae et al., 1998).

Depending on availability of data for the area of interest, the 1D velocity structure used in the EGF and HGF methods can be replaced by a 3D velocity structure. If a 3D crustal velocity structure is available along the entire wave path, the low-frequency part of the ground motion can be calculated using 3D finite difference schemes. Three-dimensional finite difference methods can combine the complex source and wave propagation for a regional 1D velocity structure with site effects calculated from a local 3D soil structure.

Dynamic ground motion simulation

In a dynamic ground motion simulation the earthquake is modelled as a propagating stress relaxation across a finite fault (Archuleta and Day, 1980; Archuleta and Fraizer, 1978). The dynamic approach is more complicated than the kinematic approach, since parameters of the stress field and rock properties are taken into account. In particular, the dynamic simulation requires a description of the fault geometry, rock properties of the medium through which the waves propagate, initial stresses on the fault and a fracture criterion. The fracture criterion is a constitutive formulation which determines when the fault slips (Harris, 2004). Therefore, the physical relationships between the important faulting parameters such as stress-drop, slip, rupture velocity and rise time are

incorporated in the dynamic simulation (Hartzell, 2005). This has an advantage when it comes to understanding the rupture dynamic and physics of an earthquake. The rupture process in dynamic modelling is initiated at the hypocenter, where the stress drops to the sliding friction value. A constant rupture velocity, for which the stress relaxation spread across the fault plane, is assumed and when the rupture front passes new areas on the fault, the area undergoes immediate stress relaxation, corresponding to the stress-drop (Archuleta and Day, 1980). The stress-drop is the change in stress from the initial value of stress on the fault to the kinetic frictional stress value (Madariaga, 1976). A challenge in dynamic simulations of earthquakes is to assign the initial stress across the fault plane. In dynamic modelling of past earthquakes (see e.g. Olsen et al. (1997) and Peyrat et al. (2001) for an example using the 1992 Landers earthquake), slip distributions obtained from waveform inversions, can be used to estimate the initial stress. This is done by calculating the change in stress across the fault due to the slip distribution and the initial stress can then be determined as the sum of the pre-existing stress field and the stress change (Olsen et al., 1997). Through the dynamic simulation, the finial stress state, the stress-drop, the final slip and the rise time across the fault can be determined.

In this study, a hybrid broadband frequency simulation technique, using a physical representation of the fault plane, is adopted. The hybrid broadband approach is preferred, since the ground motion calculated from this technique yields spectral information in the frequency range 0.1-10 Hz, covering the frequency band for which most structures are vulnerable. Therefore, the results can be used in future risk and vulnerability assessments for the areas of the case studies. 1D crustal velocity structures are used in the case studies and simulations are generally performed at bedrock level. The issue of local site effects is addressed in Section 3.5 and Paper 5.

1.2 Hybrid broadband simulation technique

In the hybrid broadband approach the strong ground motion from a finite fault rupture of a known source mechanism and seismic moment is calculated. The fault plane is defined as a rectangle and the high-slip areas across the fault plane are defined as asperities. The total ground motion for a given site is a sum of all contributions from the asperities across the fault plane, and the directional radiation of the seismic energy is taken into account by applying a frequency dependent radiation pattern. The methodology adopted in this study follows the

approach of Pulido and Kubo (2004) and Pulido et al. (2004). The ground motions are calculated for the frequency range 0.1 to 10 Hz. Ground motion simulations are calculated with waveform modelling in the frequency range 0.1-2 Hz and stochastic modelling for 1-10 Hz. In the frequency range 1.6-2 Hz the two methods overlap and are combined using a Hanning taper. The simulation results from the two simulation techniques are thereby smoothly replaced in this frequency band. A frequency dependent radiation pattern is applied in the simulation, ensuring that the theoretical double-couple for low frequencies is transformed smoothly into a uniform radiation pattern at higher frequencies.

Low-frequency ground motion simulation

The low-frequency ground motion is calculated for the frequencies 0.1-2 Hz. In the simulation of the low-frequency ground motion the fault and asperities are divided into subfaults, which are treated as point sources. The total ground motion at a site is obtained by summing point source contributions. A time delay, calculated by applying a constant rupture velocity within each subfault, is added to the simulated ground motion for the subfault, while propagating the rupture along the fault. The seismogram for each point source is calculated numerically using the discrete wavenumber theory of Bouchon (1981). From this method, the wave propagation through a flat-layered crustal velocity structure can be calculated for a known focal mechanism and source moment function. The point source moment is defined as a smoothed ramp function

$$M(t) = \frac{M_0}{2} \cdot \left(1 + \tanh\left(\frac{4 \cdot (t - \tau/2)}{\tau}\right)\right),$$

where M_0 is the seismic moment of the point source, t is the rupture time and τ is the asperity rise time (Pulido and Kubo, 2004).

In the discrete wavenumber method Bouchon (1981) showed that the Green's functions for an elastic medium, expressed as a double integral over the frequency and the horizontal wave number, can be exactly represented through a discrete summation. Applying this, a source array of an infinite number of circular sources is added to a point source at equal distance from each other. The distance between the sources controls the time the sources need to respond, and is a function of the wave velocity. From this distance, a discrete set of horizontal wave numbers is defined, and these give the solution to the numerical problem. The displacement field from an earthquake is used to calculate low-frequency

seismograms. The total displacement field is found from the superposition of the elastic wave field radiation potential from a single source. The superposition is made over the entire source array of point sources and the total radiation potential is obtained as a sum over all the individual radiation potentials from the point sources. Bouchon (1981) showed that the 1D discretization of the wave field is in good agreement with the 2D case. For this reason, it is reasonable to use the 1D method rather than the 2D method.

High-frequency ground motion simulation

The high-frequency ground motion (1-10 Hz) is calculated assuming a finite asperity model, as in the calculation of the low-frequency ground motion. The high-frequency ground motion for each point source is calculated using the stochastic approach of Boore (1983). The total high-frequency ground motion for all the subfaults is obtained by summation, following the summation approach suggested by Hartzell (1978) for the empirical Green's function method.

The stochastic simulation of high-frequency ground motion is based on seismological models of radiated spectra. The simulations are conducted both in frequency and time domain, where a suite of windowed stochastic time series is filtered, such that the amplitude spectrum equals an averaged specified spectrum (Boore, 1983). The method combines empirical and predictive techniques and only shear wave contributions are considered. Transient time series are obtained through multiplication of a target spectrum, with a preferred shape, and a spectrum obtained from a time sequence of Gaussian white noise. From this, the shape of the target spectrum is obtained and the time series are calculated by transforming the new spectrum back into the time domain.

The stochastic method requires a target spectrum, which is defined as a spectral shape function of the earthquake size and stress-drop. The cut-off frequency is assumed to be independent of the earthquake size. The seismic moment M_0, and the corner frequency f_c , are assumed to control the shape of the spectrum for different earthquake magnitudes. The parameters are related by

$$f_c = 4.9 \cdot 10^4 \cdot \beta \cdot \left(\frac{\Delta\sigma}{M_0}\right)^{1/3},$$

where β is the shear wave velocity and $\Delta\sigma$ is the stress-drop (Brune, 1970). The strength of the high-frequency radiation is thought to be controlled by the stress-drop (Boore, 1983).

The empirical Green's function method was originally given by Hartzell (1978), and has later been improved by Irikura (1986). Irikura (1986) proposed a method where ground motion from a large earthquake is represented as a superposition of the ground motion records from several small earthquakes, treating the problem as a combination of ruptures of single subfaults.

Frequency-dependent radiation pattern

In the stochastic model of Boore (1983) the average radiation pattern can differ up to 10-20%, depending on whether an equal weighting of the whole focal sphere is used, and if the root mean square or mean radiation pattern is applied. This problem was solved by Pulido and Kubo (2004) with a frequency dependent radiation pattern.

The variation of the radiation pattern for SV and SH waves is considered by Pulido and Kubo (2004), where the double-couple low-frequency radiation pattern is transformed into the isotropic high-frequency radiation pattern by a smooth transition in the intermediate frequency interval (1-3 Hz in this study). Based on this approach, the radiation pattern coefficient becomes independent of the source-receiver azimuth and take-off angle for increasing frequency (Pulido and Kubo, 2004).

The frequency dependent radiation pattern, R_{pm}, is given as

$$R_{pm}(i,\theta,\omega) = F_m(\phi,\delta,\lambda,i,\theta), \qquad \text{for } \omega \le \omega_1,$$

$$R_{pm}(i,\theta,\omega) = F_m(\phi,\delta,\lambda,i,\theta) + \left[\frac{R_{S,ave}}{\sqrt{2}} - F_m(\phi,\delta,\lambda,i,\theta)\cdot\frac{(\omega-\omega_1)}{(\omega_2-\omega_1)}\right], \quad \text{for } \omega_1 \le \omega \le \omega_2,$$

$$R_{pm}(i,\theta,\omega) = \frac{R_{S,ave}}{\sqrt{2}}, \qquad \text{for } \omega \ge \omega_2,$$

where F_m is the traditional radiation pattern coefficients for SV and SH waves, given by Aki and Richards (2002). ϕ, δ, λ are strike, dip and rake, respectively, at a receiver with take-off angle i and azimuth θ, ω is the frequency, *and* ω_1 and ω_2 are the limits to the frequency band, for which the frequency dependent radiation

pattern is used . The factor $\sqrt{2}$ comes from the partitioning of the S-wave into SV and SH. $R_{S,ave}$ is the average radiation pattern coefficient for the total S-wave. This was defined by Boore and Boatwright (1984) as

$$R_{S,ave} = \left[\sum_{m=SH,SV} \left(\frac{\int_{\pi/2}^{\pi} \int_{0}^{2\pi} F_m(\phi, \lambda, \delta, i, \theta) \sin i \cdot d\theta \cdot di}{\int_{\pi/2}^{\pi} \int_{0}^{2\pi} \sin i \cdot d\theta \cdot di} \right) \right].$$

The average radiation pattern coefficient is calculated for all rays departing from the upper focal sphere (θ=0°-180°).

The amplitude of the high frequency ground motion, A_m, including the frequency dependent radiation pattern, at a receiver is given as

$$A_m(\omega) = \frac{R_{pm}(i, \theta, \omega) \cdot M_0 \cdot S(\omega, f_c) \cdot F_S e^{-\pi \cdot \omega \cdot \Delta / Q(\omega) \cdot \beta} \cdot P(\omega, \omega_{max})}{4\pi\rho\beta^3\Delta}.$$

This is the *m*'th component of the acceleration Fourier spectrum for a point source, $S(\omega, f_c)$ is the ω-squared source model, with the corner frequency given as above. F_S is the amplification due to the free surface, Δ is the distance between the source and the receiver and $P(\omega, \omega_{max})$ is the high-frequency cut-off of the point-source acceleration spectrum (Pulido and Kubo, 2004). The hybrid broadband simulation technique was successfully validated in retrospect studies of e.g. the 2000 Tottori, Japan (Pulido and Kubo, 2004) and the 2004 Sumatra, Indonesia (Sørensen et al., 2007a) earthquakes.

1.3 Addressing the deterministic seismic hazard

In this thesis the focus is on hybrid broadband frequency ground motion simulations and the value of such simulations in seismic hazard assessment. Studies of two different tectonic regions with potential for large earthquakes have been conducted. This is meant as a comparative study of the performance of the applied simulation technique. The first case study concerns a retrospect study and the second is a predictive study for hazard assessment. The geographical focus is the region of the 2008 Wenchuan, China earthquake and the city of İzmir, located on the west coast of Turkey.

The retrospect study concerns the 2008 Wenchuan earthquake, and was motivated as a verification of the applied simulation technique. The first part of the study focuses on the performance of the hybrid broadband simulation

technique's capability to reproduce the observed ground motions. Also, the fault complexity and the availability of several fault models opens up the possibility of using different slip models in the ground motion simulations and in this way evaluate the slip models (Paper 1). The Wenchuan earthquake resulted in heavy damage and total collapse of a large number of buildings. A field trip to the earthquake affected area in October 2008 served as a basis and motivation for a reconnaissance study of the distribution of building damage and comparing this to the observed and simulated ground motions (Paper 2).

In İzmir, the main concern is to assess the earthquake hazard for the city, and this is a predictive study. No large earthquakes have occurred in this area since 1778 and the high probability of large earthquakes along faults in the vicinity of the city of 4 million inhabitants is of course a major concern. The hybrid broadband ground motion simulation technique is applied to calculate the expected ground motions from several earthquake scenarios. Due to the proximity of several large active faults to the city, the first part of the study focuses on the identification of the faults posing the largest threat to the İzmir area (Paper 3). Since the input parameters used in the scenario earthquakes are associated with large uncertainties, the variability of the simulated ground motions is investigated (Paper 4). The applied hybrid broadband simulation technique calculates the ground motion for bedrock conditions. İzmir is located on large sedimentary and fluvial deposits. Therefore, amplification of bedrock ground motion as the wave propagates through the soil column is an important aspect of the hazard assessment for İzmir. Potential of local site effects across the city has been estimated using H/V spectral ratios obtained from ambient noise measurements. Also, theoretical soil response is calculated based on modeled soil columns for the Karşıyaka district in İzmir (Paper 5).

2. The May 12, 2008 Wenchuan earthquake

On May 12 2008, a great earthquake of M_w 7.9 occurred in the Sichuan province of China. The earthquake caused more than 80,000 causalities and left more than 5 million people homeless. It is estimated that more than 5.36 million buildings were destroyed in the earthquake, and that 21 million buildings were left damaged in Sichuan and the neighboring provinces. The economic loss due to the earthquake is estimated at more than 124 billion USD (Klinger et al., 2010; USGS, 2009).

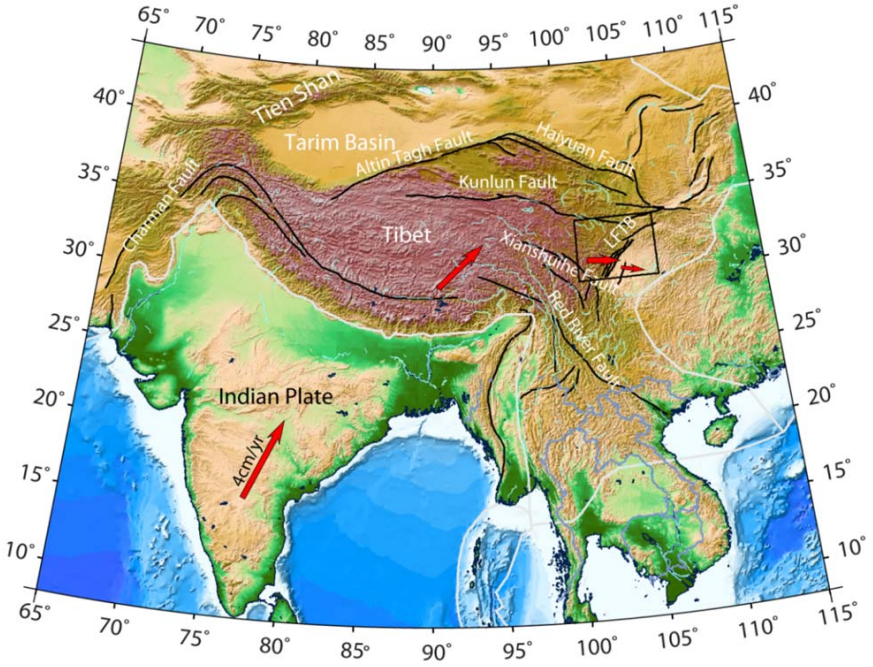

Figure 1. Tectonic setting around the Tibetan plateau situated between the northward moving Indian plate and stable Eurasian plate. Major plate boundaries are given in gray, main faults are given in black. The GPS velocities are shown as red arrows. The Longmen Shan fold-thrust belt (LFTB) is located inside the black box

The Wenchuan earthquake is one of the largest continental thrust earthquakes ever recorded and following the event lot of field measurements have been conducted. Also, due to the recent installation of the National Strong Motion Observation Network System of China (put into formal operation in March 2008) the earthquake was recorded on many near field stations.

The Wenchuan earthquake occurred along the Longmen Shan fold-thrust belt (Figure 1), where the Sichuan Basin is underthrusted by the Tibetan Plateau. The area is dominated by the collision of the northward-moving Indian plate into the stable Eurasian plate. The northward motion of the Indian plate forces the Tibetan Plateau to escape eastward; a motion which is mainly accommodated along large east-west trending strike-slip faults such as the Kunlun (left lateral) and the Xianshuihe (right lateral) faults. Across the Longmen Shan fold-thrust belt the eastward motion of the Tibetan Plateau decreases with 4 mm/yr, and the Wenchuan earthquake was a manifestation of this motion (Burchfiel et al., 2008; Chen et al., 2000; Zhao and Zhang, 1987), see Figure 1.

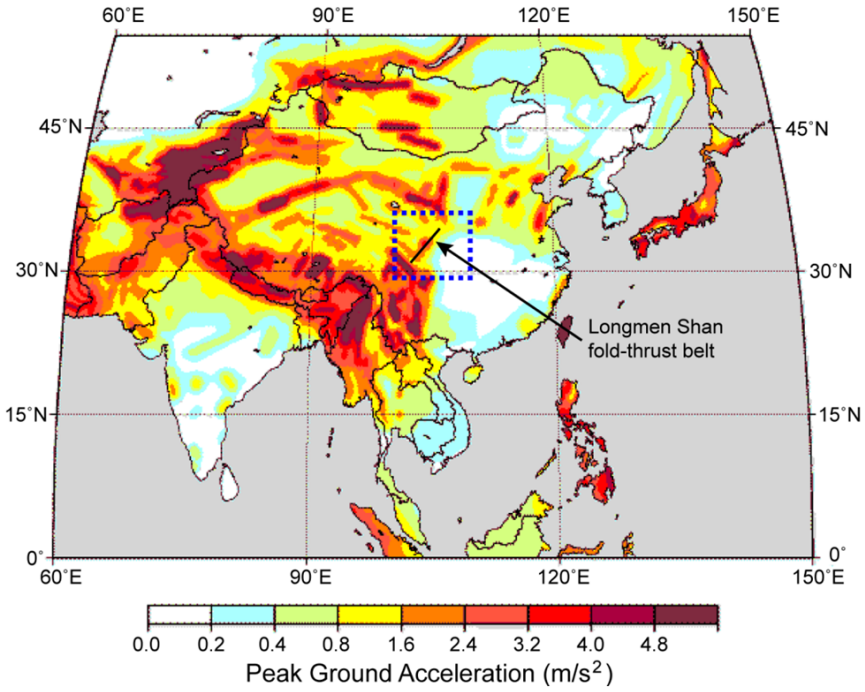

Figure 2. Probabilistic seismic hazard map of Asia. The area of the Wenchuan earthquake is within the blue dashed box and the approximate location of the Longmen Shan fold-trust belt is marked with a black line. Modified from Zhang et al. (1999). The map is made for a 475 years return period.

The seismic activity of the Tibetan plateau is known to be very high and several M>7 earthquakes have occurred along the Kunlun and Xianshuihe faults within the last century. In the period 638-1983 a total of 35 earthquakes with M>5 occurred in the Songpan-Longmen Shan region. Among these were an earthquake of M 7.5 in 1933 in Diexi (north of the epicenter of the Wenchuan earthquake) and two M 7.2 events occurred within a week in 1976 near Songpang (140 km north of the Wenchuan earthquake) (Zifa, 2008). According to the seismic zonation map of China, the largest expected earthquake along the rupture zone of the 2008 Wenchuan event was an M 7.3 (Zifa, 2008). Figure 2 shows the probabilistic seismic hazard map of Asia from GSHAP (Global Seismic Hazard Assessment Program). Maximum expected ground motion along the Longmen Shan fold-thrust belt were estimated to be about 3.2 m/s^2 for a return period of 475 years (Zhang et al., 1999), which is a much lower value than the ground shaking levels observed during the 2008 Wenchuan earthquake.

The rupture of the Wenchuan earthquake started in the south and propagated northward for approximately 300 km. The most southern part of the rupture had thrust mechanism, while the northern segment ruptured predominantly as strike-slip. Acceleration levels of up to 1 g were recorded (Li et al., 2008a). Several parallel fault strands are expected to have ruptured during the earthquake and vertical displacements of 4-5 m, together with dextral displacements of up to 2 m, were reported at the surface along these fault strands (Lin et al., 2009).

Several slip distributions obtained from different waveform inversions of teleseismic data, have been published following the event (Ji and Hayes, 2008; Koketsu et al., 2009; Nakamura et al., 2009; Nishimura and Yagi, 2009; Wang et al., 2008; Zhang et al., 2008; Zhao et al., 2010) (see Figure 3 and Figure 3 of Paper 1). The main uncertainty among the different source models are the amount of slip and the location of asperities. The models of Nakamura et al. (2009), Zhao et al. (2010), Wang et al. (2008), Koketsu et al. (2009) and Nishimura and Yagi (2008) all agree on one primary asperity located in the southern to central part of the fault. The model by Zhang et al. (2008) agrees with a high-slip asperity close to the epicenter, but this model obtains a rupture of the fault up to 200 km south of the epicenter, and estimates a total fault length of 500 km along strike. The model from Wang et al. (2008) comprises of several subevents, and it is the only model which contains clearly separated asperities on three individual fault segments along different parallel fault strands. This model is also the only model that is obtained from a combination of waveform inversion and local coseismic displacement from GPS. The amount of maximum slip from the models is in the

range of 5 to 10 m, where the largest slip is found for the slip models using a narrow fault plane.

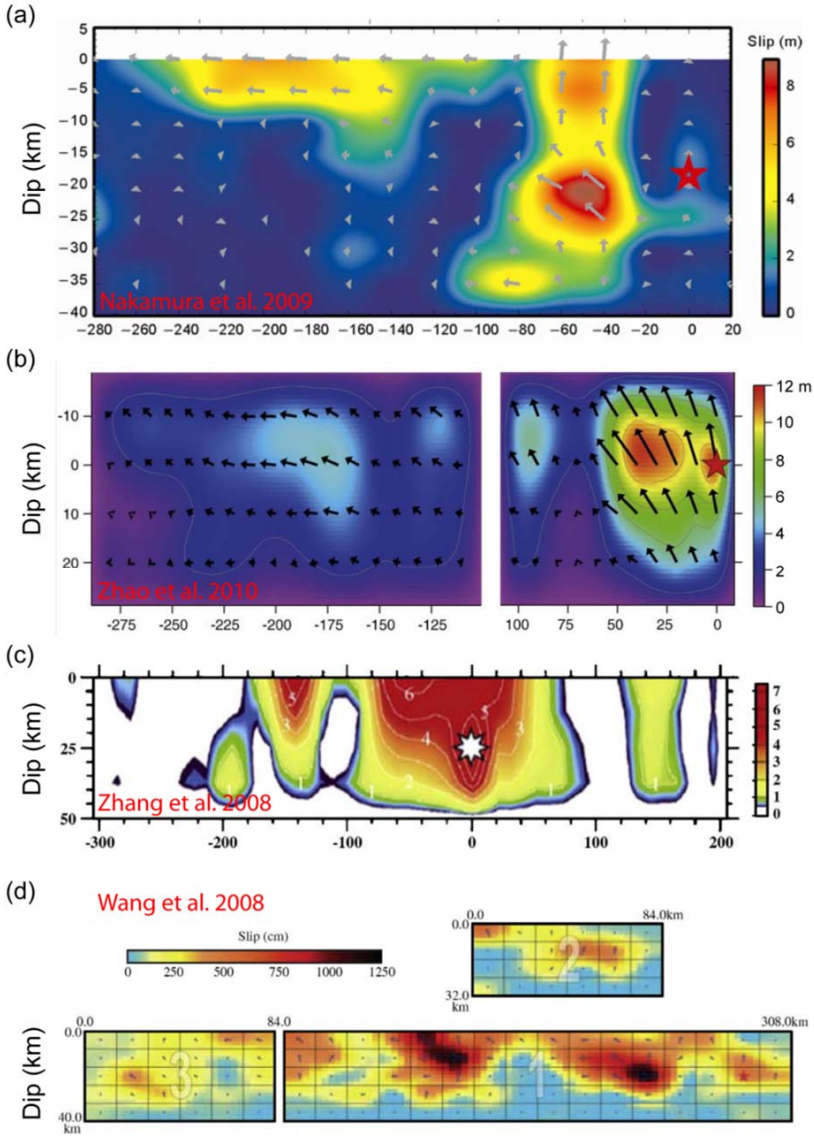

Figure 3. Slip distributions for the Wenchuan earthquake. Modified from a) Nakamura et al. 2009, b) Zhao et al 2010, c) Zhang et al. 2008 and d) Wang et al. (2008). Notice, the slip models are not at the same scale, and the width of the different faults are approximately the same. The length of the faults also vary, with the longest being the model from Zhang et al. (2008), which is 500 km along strike, whereas the others are approximately 300 km along strike. The segment "2" in d) is modeled for a fault strand parallel to segment "1".

2.1 Modeling ground motion for the Wenchuan earthquake

The ground motions during the Wenchuan earthquake were modeled using the simulation technique described in Section 1.2. To constrain the asperity geometry on the fault plane, three different slip models were used. By applying three models, the effect of the slip models on the calculated ground motions could be compared. This approach also opened up for a possible evaluation of the slip models based on the simulated ground motion. The slip models used are shown in Figure 3 of Paper 1 and are from Koketsu et al. (2009), Ji and Hayes (2008) and Nishimura and Yagi (2008).

The slip model from Koketsu et al. (2009) is 310 km long and 40 km wide. The model is divided into two segments, representing the southern segment of thrust mechanism and the northern segment with strike-slip mechanism. The asperity with the largest displacement is located in the southern end, with maximum displacement of 9 m. The slip model from Ji and Hayes (2008) is 315 km long and 40 km wide. The largest slip is located in the central part of the fault, with maximum displacement estimated to be 9-10 m. The slip model from Nishimura and Yagi (2008) is 320 km long and 80 km wide. This model has two primary asperities located close to the top of the fault plane. For the southernmost asperity a thrust mechanism is identified, while the northern asperity, is of strike-slip mechanism. The maximum displacement in this model is 7 m. This slip model best corresponds to field observations of surface displacement following the earthquake. Details on the input parameters used in each of the earthquake simulations are summarized in Table 2 of Paper 1.

The distribution of the simulated ground motion on the bedrock level from the three earthquake scenarios is shown in Figure 4. In all three scenarios the largest simulated ground motions are above the fault plane and associated with the location of the asperities. The simulation results from the scenarios based on the models from Koketsu et al. (2009) and Ji and Hayes (2008) show very similar distributions of both peak ground acceleration (PGA) and velcocity (PGV). Also, the calculated ground shaking levels agree well with observed ground motions. In the simulation based on the model from Nishimura and Yagi (2008) the ground motion levels are not as high as in the other scenarios. With a fault model which is twice as wide as the two other models, the scenario based on the model from Nishimura and Yagi (2008) has a stress-drop much lower than in the other models. This can explain the lower ground motion values.

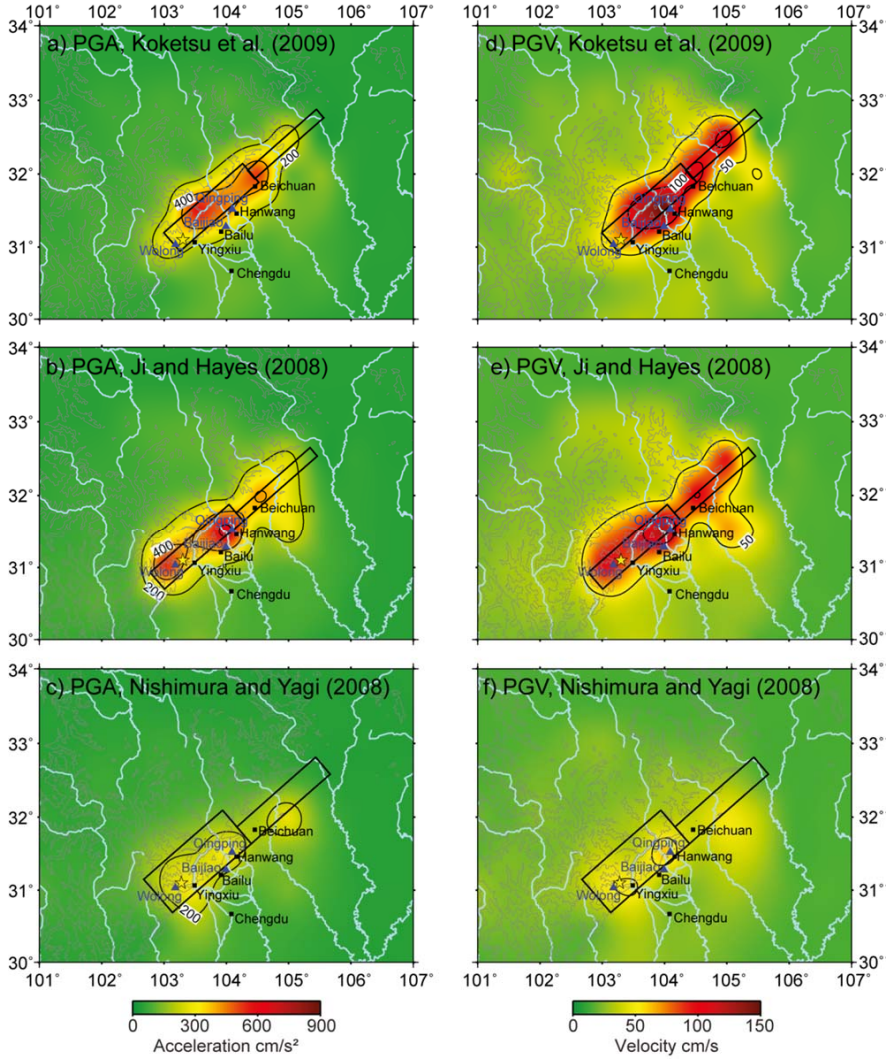

Figure 4. Simulated PGA (a-c) and PGV (d-f) distribution from the scenario earthquakes based on three different finite fault-slip models. Black boxes show the surface projection of the ruptured fault and the star, triangles and black squares show the epicenter, locations of seismic stations and cities, respectively.

The finite fault slip models from Koketsu et al. (2009), Ji and Hayes (2008), Nakamura et al. (2009), Zhao et al. (2010), Zhang et al. (2008) and Wang et al. (2008) all have widths along dip of 40-50 km. Also, a study on the fault geometry in the area by Hubbard and Shaw (2009) suggests a rupture width of approximately 40 km. Considering the very low slip predicted in the deeper part

of the fault plane in the slip model from Nishimura and Yagi (2008), the ground motions were calculated for another scenario. In this scenario the slip model from Nishimura and Yagi (2008) was reduced to only contain the upper 40 km.

The results of the simulation with the modified slip model from Nishimura and Yagi (2008) is shown in Figure 5. From the simulation much larger ground motion levels than the scenario earthquake, where the fault width was set to 80 km were obtained. Also, above the northernmost asperity the simulation produces larger ground motions, which are similar to the simulated ground motions based on the slip models of Koketsu et al. (2009) and Ji and Hayes (2008), but with slightly higher ground motion levels.

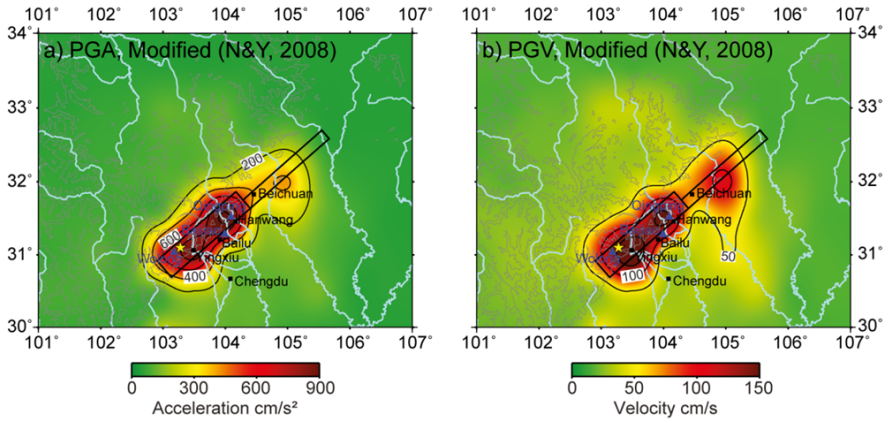

Figure 5. Simulated ground motion distributions based on the modification of the model from Nishimura and Yagi (2008). Black boxes show the surface projection of the ruptured fault and the star, triangles and black squares show the epicenter, locations of seismic stations and cities, respectively.

The simulated ground motions from all the earthquake scenarios are found to be lower than the values measured during the event. It is nevertheless important to keep in mind that site effects are not included in the simulation. Located in the boundary zone between the Sichuan Basin, approximately 500 m above sea level, and at the eastern margin of the Tibetan Plateau, with local peaks of up to 4000 m above sea level, many steep mountain sides are present. The mountain peaks are associated with focusing of seismic energy, while deep valleys between the mountains are expected to be filled with loose sedimentary material and fluvial material from the river systems. Therefore, site effects have an important role in the area, and such effects can change both the ground motion level, as well as the predominant frequencies of the ground shaking.

The intensities of the simulated ground shaking were estimated using the relations from Wald et al. (1999) to be IX or above for the majority of the fault length. Although such relations have large uncertainties and therefore should be applied with caution, this gives a rough estimate of the expected near-field intensities. For the near field area the intensities of the simulated ground motions (see Figure 20 of Paper 1) are found to be similar to those reported by the China Earthquake Administration. Away from the fault, the intensities based on the simulated ground motions are very low. This is due to the applied simulation technique which does not reproduce surface waves well, and these are dominating at larger distances.

2.2 Reconnaissance visit to the earthquake affected area

A field reconnaissance trip to the rupture area of the Wenchuan earthquake on October 18 and 19, 2008 served as a basis for discussing the damage distribution after the earthquake. In addition to the very strong ground shaking, the Wenchuan earthquake triggered more than 15.000 secondary effects, as landslides, rock falls, debris flow and mudslides. The secondary effects alone are estimated to have caused more than 20.000 fatalities (Yin, 2008). Taking the mountainous landscape, strong ground shaking, landslides and rock fall into account, it is evident that poor building practices and the mentioned secondary effects contributed to the very large human and economic consequences following the earthquake.

During the field reconnaissance trip, the cities Yingxiu, Bailu, Hangwang and Beichuan, all located along the surface rupture, were visited; all located in the direction of rupture directivity (see Figure 2 of Paper 2 for locations). Yingxiu is located in the area of the rupture initiation. The building stock in the cities along the fault had a high concentration of reinforced concrete structures with brick infill and non-engineered adobe structures. Damage observed was both of non-structural and structural nature, and many buildings had experienced soft story collapse, due to failure or partial failure of columns. The fault scarp was visible in all the visited cities, and in Bailu it ran in-between two school buildings, with a vertical offset of up to 2 m (Figure 6a).

Figure 6. Pictures taken during the field reconnaissance trip in October 18 and 19, 2008. a) Fault scarp in Bailu, b) Yingxiu, c) Hangwang, d) rock fall in Beichuan, e) material carried the debris flow in Beichuan.

Generally, damage and total collapse of structures were observed across large areas within the cities. Especially in Yingxiu and Hangwang (Figure 6b and c) the damage was widespread and buildings of both newer and older construction practice were affected. The structures still standing after the earthquake were all newer reinforced concrete buildings. The buildings sustaining the ground shaking most probably fulfill the construction requirements of newer building codes. In central Yingxiu, approximately 80% of the buildings collapsed during the earthquake (Figure 6b). Correspondingly, in the central part of Hangwang, 90-95% of the buildings were totally or partially collapsed in an area of approximately 3 km^2 (Figure 6c). The very widespread damage in Yingxiu and Hangwang, compared to Bailu might be explained by the very high ground shaking levels for the two sites. While for Bailu a maximum ground motion of 633 cm/s^2 was reported, the maximum observed ground motion close to Hangwang was more than 800 cm/s^2 (Li et al., 2008b). No records are available for Yingxiu,

but with a very short distance to the rupture initiation point and the proximity to the main asperity of the fault plane (Figure 3 in this text; Figure 3 of Paper 1; Figure 2 of Paper 2), this area experienced very high ground motions during the earthquake.

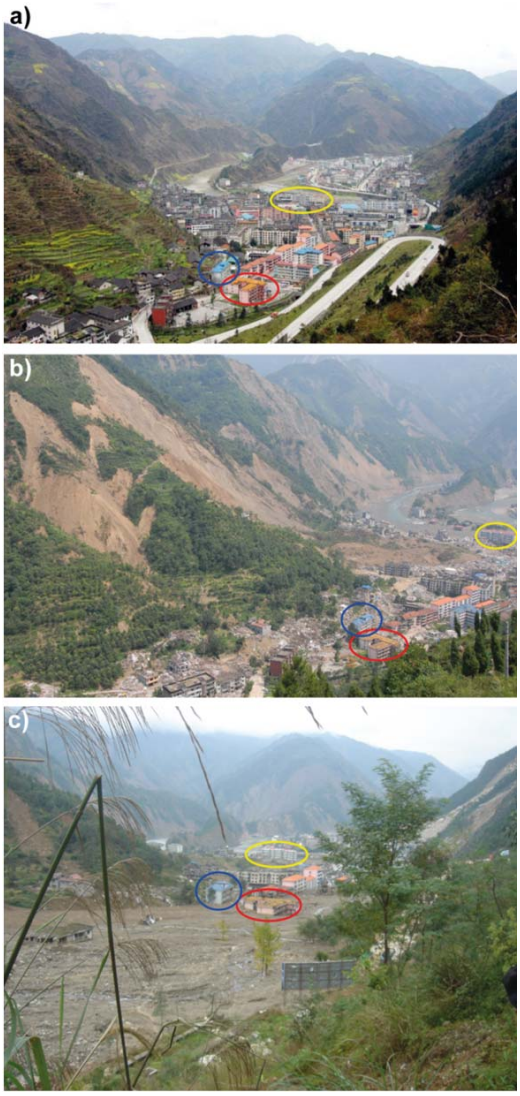

Figure 7. Overview of Beichuan. a) Photo of Beichuan before the Wenchuan earthquake (photo source unknown). b) Photo of Beichuan, taken in July 2008, after the Wenchuan earthquake. (Photo by Dr. Gonghui Wang, Kyoto University, Japan). a) and b) are from the homepage of USGS Landslide Hazard Program (2009). c) Photo of Beichuan taken in October 2008, after the debris- and mudflow. Houses are identified with colored circles on the three pictures.

The damage in the city of Beichuan differs from the other cities visited, since the city was located in a very narrow valley between steep mountains. Following the earthquake, several large landslides and rock falls were triggered, causing additional damage (Figure 6d). Furthermore, following the earthquake in May 2008, the city experienced a large debris- and mudflow in September 2008 (approximately one month prior to the field reconnaissance trip) (Figure 6e). The maximum ground motion observed near Beichuan was about 350 cm/s^2 (Li et al., 2008b). This is significantly lower than for the other visited cities. However, especially two landslides, triggered by the ground shaking, caused heavy damage to the city. During the visit, damage due to the ground shaking was evident from structural damages in the areas of the city not affected by landslides or the debris flow. In Figure 7, three pictures of Beichuan, taken from approximately the same position, are compared. The first picture was taken before the earthquake, the second picture after the earthquake and the third picture was taken after the debris flow. It is seen that many of the structures sustained the ground shaking, and are still standing following the earthquake (comparing Figure 7a and b, three building have been matched with color circles for comparison), while buildings close to the mountain sides have suffered more damage due to landslides. From the picture taken following the debris flow (Figure 7c), a thick layer (up to 3 m) of debris material and mud covering the entire southern part of the city is visible. The force of this event caused additional damage to the structures in the area.

Comparing the damage distribution in the visited cities along the fault, with simulated ground motions shows that strong ground shaking during the earthquake, combined with unfavorable frequency distribution of the ground shaking, have led to collapse of many structures. The simulated ground motions were found to have a broader peak of the most significant ground shaking in the acceleration spectra, compared to the recorded signals (Li et al., 2008a) (Figure 14 of Paper 1). However, the frequency band is overlapping, and the difference in the frequency band can be caused by site effects, which are not included in the ground motion simulations.

2.3 Other simulation studies of the Wenchuan earthquake

The Wenchuan earthquake has been simulated and presented by various authors, using some of the simulation techniques mentioned in Section 1.1 of this thesis. Paper 1 was published in the special issue on the Wenchuan earthquake of Bulletin of Seismological Society of America (BSSA) in autumn 2010. In the

following a short overview is given of the other studies presented in the BSSA special issue, treating the simulation aspect of the Wenchuan earthquake (Chavez et al., 2010; Ghasemi et al., 2010; Kurahashi and Irikura, 2010). The studies are listed in Table 1.

Table 1. Overview of the simulation studies of the Wenchuan earthquake, presented in the special issue on the event of BSSA, 2010.

Authors	**Method**	**Slip model(s)**
Chavez et al.	3D wave propagation, finite difference	Ji and Hayes (2009)
Ghasemi et al.	Stochastic	Koketsu et al. (2008) Random model
Kurahashi and Irikura	Hybrid: Low-frequency: discrete wave number method. High-frequency: EFG	Southern segment from Koketsu et al. (2009)

Chavez et al. (2010) conducted a three dimensional wave propagation modeling study, where low-frequency synthetic seismograms were calculated. The modeling was based on the staggered finite-difference method by Madariaga (1976). The input required in the modeling includes geometric and mechanical properties of the physical domain, seismic source description (strike, dip, rake and slip) and spatial and temporal discretization parameters. The focal mechanism from Ji and Hayes (2008) were adopted and the slip distribution was converted into a moment rate distribution, used as the seismic source in the finite-difference code. A thrust mechanism along the entire fault was assumed. The simulation results were compared with recordings from four stations of different epicentral distance. Also, comparison with surface differential radar interferometry (DinSAR) ground deformation imagery was included as well as a comparison of the 3D synthetic velocities with the observed intensities on the Modified Mercalli Intensity scale. Furthermore, 3D visualizations of the low-frequency synthetics were given.

In the study by Ghasemi et al. (2010) the stochastic finite-fault method of Beresnev and Atkinson (1997; 1998) has been used to simulate the ground motions of the Wenchuan earthquake. Two different finite-fault slip models; one being the model of Koketsu et al. (2008) and the other being a model, where the slip is assigned randomly by the simulation code, were assumed. In the applied

simulation technique, effects of the finite source, wave propagation path and local site effects were taken into account. However, the soil-station average transfer functions applied in the calculations were derived for California in lack of detailed information on the local site conditions. The simulation results were compared to recorded data with comparison of seismograms and both 5% damped pseudo acceleration response spectra and Fourier amplitude spectra. Also, bias and standard deviation of the response spectra were calculated for each model.

Kurahashi and Irikura (2010) simulated the Wenchuan earthquake with a hybrid method. The results were analyzed for the low-, high- and in the broadband frequency domain. The low-frequency ground motions were obtained numerically using the Discrete Wave Number method (Bouchon, 1981), while the high-frequency ground motions were obtained by applying EGF. Since no records of aftershock of the Wenchuan earthquake were available, the EGF are taken from an aftershock following the 2008 Iwate-Miyagi Nairiku earthquake in northeastern Japan which had a similar focal mechanism as the Wenchuan earthquake. The path propagation effect and the site effects from the aftershock record were removed following Iwata and Irikura (1999). The slip model used in the simulation was from Koketsu et al. (2009). However, only the southern part of the model was used in the scenario, and only the asperities were included. It was consequently assumed that the ground motions were only generated from the asperities based on an analysis of seismograms from six stations, from which the distance to the asperities from the epicenter was also determined. The simulation results were compared to seismograms in three frequency bands, acceleration response spectra and pseudo velocity spectra.

Several assumptions and simplifications to the rupture and source model are made in the simulation studies of the Wenchuan earthquake. Also, site effect estimations are excluded or only considered to some extent in the studies. Nevertheless, all the above mentioned simulation studies manage to some extent to reproduce the ground motion characteristics observed during the Wenchuan earthquake.

The amplitudes and polarities of the seismograms obtained from Chavez et al. (2010) vary from the observed ground motion. However, especially for the far field station, very close estimates of the Fourier Amplitude spectra were obtained in this study. Also, from the 3D visualization of the low-frequency synthetic velocities, a clear pattern of directivity along the fault is obtained. This can partly explain the heavily damaged area along the fault, while the degree of building damage was less extensive in a close distance perpendicular to the fault. The

maximum synthetic velocity propagation pattern can to some extent be compared with the observed Modified Mercalli Intensities in the near field area. However, the ground motion level is under-estimated significantly for the epicentral area.

The results from Ghasemi et al. (2010) give slightly higher PGAs than observed during the earthquake on several of the stations, and the shape with several wave packages is not clearly seen in the synthetic seismograms. As the case for Chavez et al. (2010) the Fourier spectra and the spectral acceleration are generally in good agreement with the spectra of the observed data. The model tends to over predict the ground motion in the period range 1-4 s (Figure 11 of Ghasemi et al., 2010).

In the study by Kurahashi and Irikura (2010) the amplitudes of the synthetic waveforms, from the high-frequency ground motion modeling, tend to be overestimated and under-estimated in the backward and forward directivity direction, respectively. In the comparison of the acceleration response spectra and pseudo velocity spectra a general agreement of the frequency content of the simulated and observed waveforms is observed. The simulation procedure for the high frequencies in this study can be spurious. EGF is a well know method to simulate ground motions. By adopting aftershocks from the rupturing fault as the EGF, propagation path effects and local site effects are taken into account in the ground motion simulation. However, a requirement for using EGF is, as stated in Section 1.1, that the aftershocks adopted as EGF must be recorded at the same station as the main event. One could argue that since Kurahashi and Irikura (2010) adopt an aftershock from a Japanese earthquake as EGF for the simulating the Wenchuan earthquake, and afterwards remove the propagation path effect and site effects, the authors could instead have used synthetic/theoretic Green's functions (HGF) in their calculations.

Based on this review of ground motion simulation studies of the Wenchuan earthquake, it is evident that the simulated ground motion techniques to a large extent succeed in reproducing the observed frequency content and spectral levels. However, an exact representation of the waveforms for a broadband frequency interval is somewhat more difficult to obtain. This was also found in the ground motion simulations presented in Sections 2.1 and 2.2, where the general frequency content of the ground shaking was obtained, while the recorded waveforms were difficult to reproduce.

3. Seismic hazard assessment for İzmir

The predictive part of this thesis concerns the city of İzmir, which is the third largest city of Turkey with approximately 4 million inhabitants. Located within the Aegean-Anatolian region, İzmir is situated in one of the most seismically and tectonically active regions in Europe.

İzmir is located close to several faults, which are reactivated through regional deformations, associated with the westward migration and rotation of the Anatolian microplate. The city is therefore characterized by significant seismic hazard, and destructive earthquakes have occurred in historical times, most recently in 1778. This event followed two preceding earthquakes, separated in time by approximately 50 years (Ambraseys and Finkel, 1995; Papazachos and Papazachou, 1997; Papazachos et al., 1997).

Several large industries and the largest harbor in western Turkey are located around İzmir Bay. In this respect, the city is an economically important center. In order to be able to mitigate the seismic risk in the city, thorough and reliable information is needed about the seismic hazard. The most densely populated areas within İzmir are located on unconsolidated sediment deposits from river deltas. These deposits are expected to amplify ground shaking during an earthquake, and site effects are therefore important to consider when assessing the seismic hazard.

The seismic hazard assessment for İzmir, presented in this study, is divided into three parts. First, the active faults that control the seismic hazard in İzmir are identified through ground motion simulations of earthquake rupture scenarios on several of the faults in the vicinity of İzmir. Second, the uncertainties in the simulated ground motions due to uncertainties in the input parameters are considered. Third, expected ground motions are estimated taking into account the effect of soil deposits, using the simulated ground motion for bedrock level and transfer functions obtained as H/V spectral ratios from ambient noise measurements. In order to give a framework for the study, a description of the tectonic setting and seismicity as well as previous hazard estimates for the area are given.

3.1 Tectonic setting and seismicity of western Turkey and İzmir

The regional deformation of the Aegean-Anatolian region is dominated by the collision of the African and Arabian plates with Eurasia, the collision between north-western Greece and Albania with the Apulia-Adriatic platform and the Hellenic subduction zone in the south (Taymaz et al., 1991) (Figure 8). The collision of the Arabian plate with Eurasia causes westward migration of the Anatolian microplate, a motion which is accommodated along two large strike-slip faults, the North Anatolian (right-lateral) and the East Anatolian (left-lateral) faults. The African plate subducts underneath the Aegean Sea along the Hellenic arc, and causes backarc extension. This is explained as a combination of slab-roll back of the African plate, gravitational collapse of over-thickened crust, westward extension of the Anatolian plate and south-west movement of the Greek block relative to Anatolia (Jolivet, 2001 and references therein; Taymaz et al., 2007). Evidence of the occurrence of backarc extension is seen as east-west trending graben structures, such as the Gulf of Corinth, the Gediz Graben and the Büyük Menderes Graben, which are present on either side of the Aegean Sea. The regional tectonic setting is summarized in Figure 8.

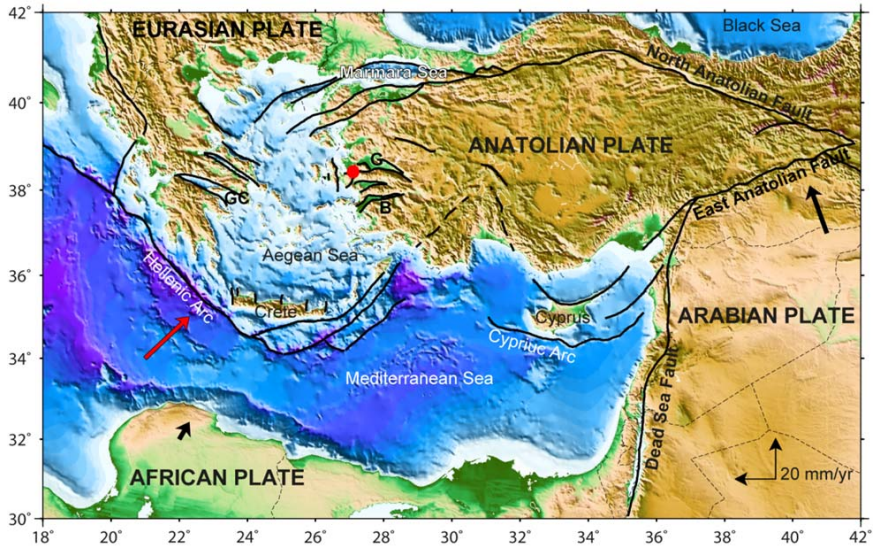

Figure 8. *Tectonic map of the Aegean-Anatolian region. Solid black lines show faults and plate boundaries, modified from Bird (2003), ten Veen (2004) and McClusky et al. (2000). Heavy black arrows show the plate motions of the African and Arabian plates relative to a stable Eurasia, the red arrow gives the plate motion of the African plate relative to a stable Anatolian plate. All plate motions are taken from the NUVEL 1A reference model (DeMets et al., 1990). Locations of the main structures are given as follows: GC, Gulf of Corinth; G, Gediz Graben; B, Büyük Menderes Graben. The location of İzmir is marked with a red dot.*

The seismicity around the Aegean Sea is dominated by thrust mechanisms of the earthquakes along the Hellenic Arc and along the west coast of Greece and Albania, with some strike-slip and normal fault mechanisms (Figure 9). Strike-slip mechanism earthquakes occur along the westernmost part of the North Anatolian Fault and its continuation into the northern Aegean Sea. Along the east coast of Greece and the west coast of Turkey, normal faulting earthquakes indicate extension of the landmasses. Active faults and focal mechanisms for the area around the Aegean Sea are shown in Figure 9.

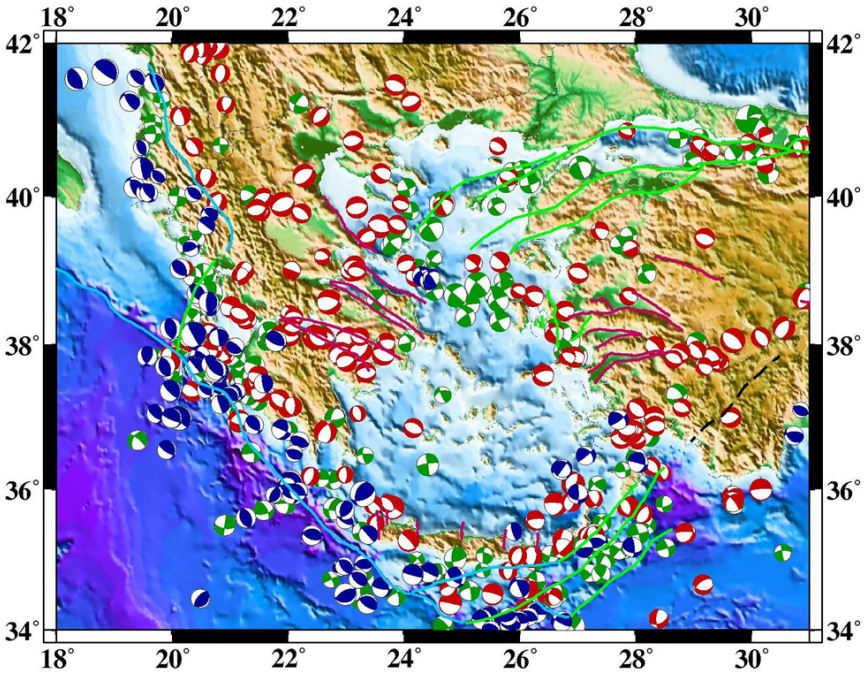

Figure 9. Active faults and earthquake focal mechanisms in the Aegean region. Red, green and blue symbols are used for normal faulting events and faults, strike-slip faulting events and faults and thrust faulting events and fault, respectively. The fault plane solutions are compiled from the INGV, USGS and Global CMT databases.

Several GPS studies have been conducted for the Aegean-Anatolian area in order to map the plate velocity and deformation (McClusky, 2000; Nyst and Thatcher, 2004 and references therein) (Figure 10). These studies confirm westward migration of the Anatolian plate. A change in the velocity field is identified in western Turkey and the Aegean Sea. McClusky et al. (2000) showed a clear increase in the plate velocity of the Anatolian microplate from the east to the west, confirming extention. There is a stable westerly orientation in eastern and

central Turkey, while a counter-clockwise rotation was found in the Aegean area, see Figure 10. A similar picture of the deformation in the Aegean Sea and surroundings was obtained by Nyst and Thatcher (2004). The change in the orientation of the velocity field is located in the area around İzmir.

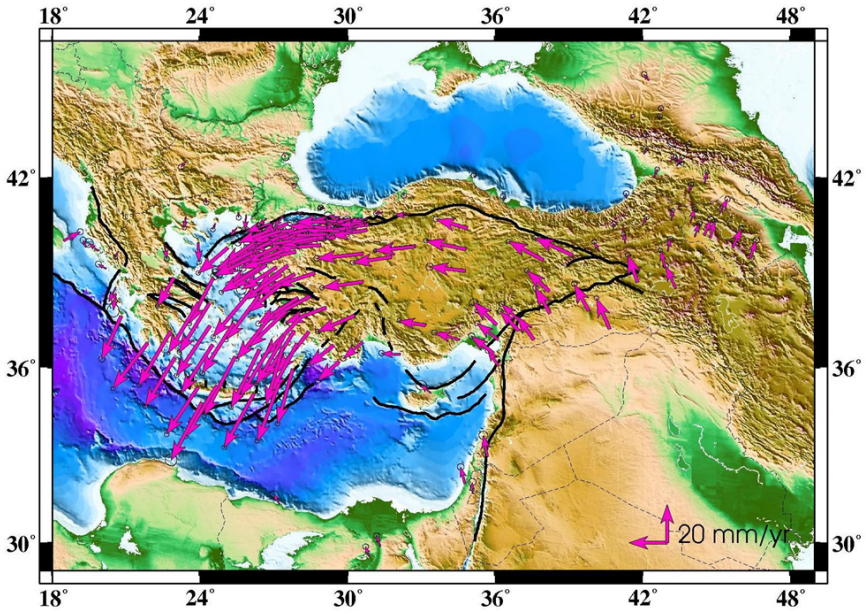

Figure 10. GPS horizontal velocities and 95% confidence ellipses in a Eurasia-fixed reference frame from 1988-1997, data plotted is from McClusky et al. (2000). The plate boundaries and faults from Figure 8 are also shown.

Counter-clockwise rotation of western Anatolia causes the reactivation of several faults around the city of İzmir. Active faults in the vicinity of İzmir have been mapped by Emre et al. (2005) and reactivation of these and new developing structures became evident during an earthquake swarm south-west of İzmir in 2005, when three $M_w > 5.3$ events occurred within three days (Benetatos et al., 2006).

The change in the regional velocity field in the area around İzmir has been investigated in detail by Aktuğ and Kılıçoğlu (2006) with a local GPS study focusing especially on three large faults: İzmir fault (striking east-west, located underneath İzmir), Tuzla fault (striking southwest-northeast, located southwest of İzmir) and Gülbahçe fault (striking north-south, located west of İzmir), see Figure 11. The detailed GPS study mapped small-scale block rotations and differences in relative velocities on both side of the faults, which are found to be

significant, especially for Seferihisar and Tuzla faults. Continuous opening of İzmir Bay is confirmed in this study by increasing velocities from the north to the south.

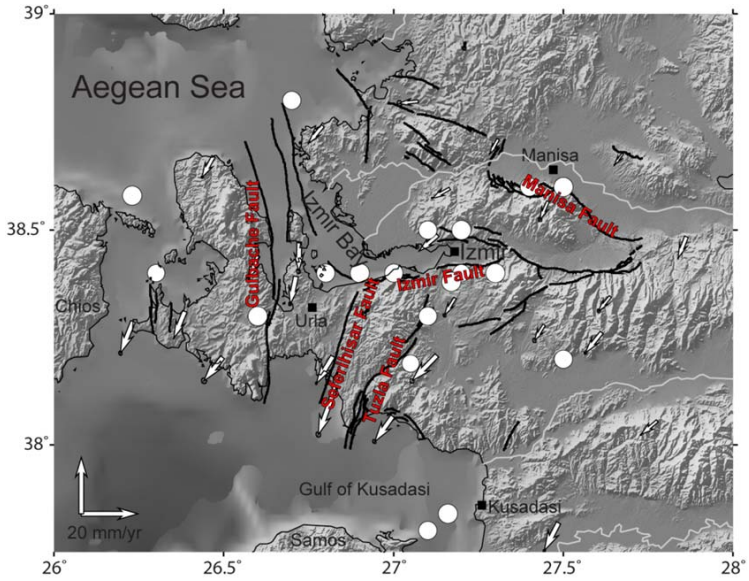

Figure 11. Map of the area around İzmir. Faults are given as thick black lines, and names are given in red font (Emre et al, 2005). The historic earthquakes in the area are indicated as white circles (Ambraseys and Finkel, 1995; Papazachos and Papazachou, 1997; Papazachos et al., 1997) and the GPS velocity field from Aktuğ and Kılıçoğlu (2006) is shown as white arrows.

İzmir and its surroundings are known to have experienced destructive earthquakes several times in recent history. The most significant events in the historical records are shown in Figure 11. The record of the historical events indicates that İzmir and Tuzla faults are the two most active faults in the area (Ambrasey and Finkel, 1995; Papazachos and Papazachou, 1997; Papazachos et al., 1997).

The latest large earthquake in İzmir occurred in 1778 with estimated M_w 6.4. This event was preceded by two previous earthquakes in 1688 (M_w ~6.8) and 1723 (M_w ~6.4). The close spacing in time of the three large events can possibly be explained by coupling between faults and stress transfer. The three earthquakes all caused extensive damage in İzmir. The 1688 event is reported to be a locally very destructive event, with the most significant damage in the low lying areas. Three-quarters of the houses and public buildings were heavily damaged, on the verge of collapse, if not completely collapsed in the event. The sea shore was

reported to advance inland due to ground sinking of approximately 60 cm, and it was estimated that about 5000 people were killed (Ambraseys and Finkel, 1995). Following the 1778 earthquake, large parts of İzmir were almost totally ruined and the buildings left standing were on the verge of collapse. Also in this earthquake, the ground sunk, changing the shoreline. More than 200 people were killed in this earthquake (Ambraseys and Finkel, 1995).

During the last 230 years no large earthquakes have occurred in the area close to İzmir. Considering the velocity differences across the faults identified by Aktuğ and Kılıçoğlu (2006), large stresses are expected to have built up across the faults. The faults around İzmir are therefore considered to be loaded and prone to rupture in the near future.

3.2 Previous seismic hazard assessments for İzmir

Previous seismic hazard analyses for İzmir and the surrounding area have been conducted on a regional scale and more local scale. All the previous hazard estimates are probabilistic studies, and the methodology applied in this study therefore differs from the previous estimates.

On a regional scale the probabilistic seismic hazard of western Anatolia has been addressed in the GSHAP project (Gardini et al., 1999) and in the SESAME project (SEismotectonic and Seismic hazard Assessment of the MEditerranean) (Jimenez et al., 2003). With a return period of 475 years (10% probability of exceedance in the ground motions in 50 years) the two studies predict PGAs of 0.3-0.5 g for bedrock conditions. Since the studies are regional, no details can be related to specific faults around İzmir. Only larger scale structures, such as the North Anatolian fault and the Hellenic Arc have a clear expression on the map.

On a local scale, two probabilistic studies address the seismic hazard of İzmir (Deniz et al., 2010; MMI, 2000). The probabilistic seismic hazard assessment from the İzmir Earthquake Master Plan (MMI, 2000) reports expected PGAs for bedrock conditions with a 475 year return period to be 0.2-0.4 g, and slightly larger for soft soil conditions. Deniz et al. (2010) obtain similar values (0.3-0.4 g) for rock sites. These values are in agreement with the regional studies.

3.3 Ground motion simulations on faults near İzmir

The first step in the deterministic seismic hazard assessment for İzmir was to identify which of the faults in the vicinity of the city that controls the largest seismic hazard. A rupture along the surface rupturing İzmir fault, located along the southern coast of İzmir Bay, will obviously cause large ground deformation and strong ground shaking in İzmir. The objective of Paper 3 is to estimate bedrock ground motion levels in İzmir for ruptures along several of the active faults, and from that identify the possible earthquake ruptures that pose the largest threat. The applied simulation approach is described in Section 1.2.

Figure 12. Map showing the simplified faults for which ground motion simulations were conducted. The codes for the various scenarios are written in blue next to the respective faults.

Nine earthquake rupture scenarios were defined along the largest faults in the area (Figure 12). Scenarios 1A-C and 5A-C are along İzmir and Manisa faults, respectively. These are normal faults, and large vertical offsets (>40 m) are visible on the surface for both faults. For İzmir fault three scenarios were defined; corresponding to a rupture of the western segment, the eastern segment and a combination of both. For Manisa fault, three earthquake scenarios were defined on different segments of the fault. Scenarios 2 GF, 3 TF and 4 SF are earthquake

ruptures along Gülbaçhe, Tuzla and Seferihisar faults, respectively. All these are strike-slip mechanisms. The source parameters for the nine earthquake scenarios are summarized in Table 1 of Paper 3.

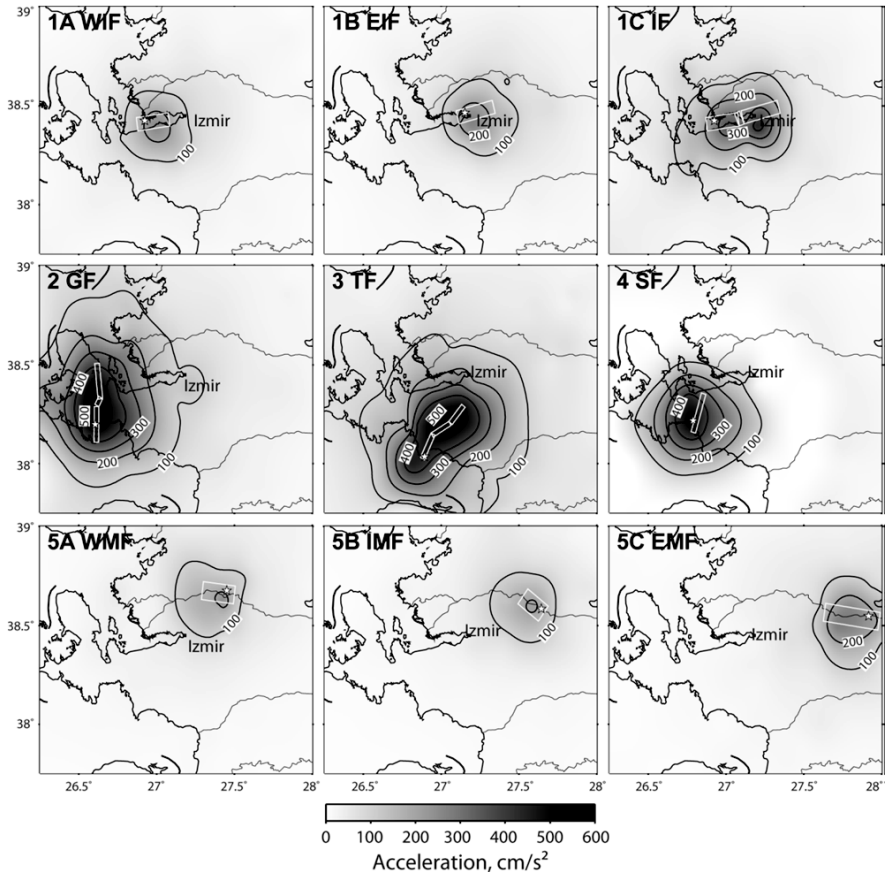

Figure 13. PGA distribution of the nine earthquake scenarios on active faults in the vicinity of İzmir. White boxes show the surface projection of the ruptured fault plane.

The simulation results, in terms of PGA distribution, from all nine earthquake scenarios are shown in Figure 13. The largest ground motions were simulated for the scenarios along Gülbaçhe, Tuzla and Seferihisar faults. However, the largest ground motions in the center of İzmir were found from the earthquake scenario along İzmir fault. The waveform of the longest duration in the center of İzmir was also found for this scenario. In the earthquake scenario along Tuzla fault the rupture initiation point was located in the southern end of the fault. The rupture of the scenario therefore propagated towards İzmir, and increased peak ground motion levels, with a shorter duration, were observed to the north of the fault

and in İzmir. Based on the nine earthquake scenarios, it was concluded that rupture along İzmir and Tuzla faults pose the largest threat, in terms of ground shaking to İzmir.

3.4 Effect of parameter uncertainty on simulated ground motions

The results from Paper 3 gave the expected ground motion distributions based on earthquake scenarios along various faults. However, the input parameters adopted for the scenario earthquakes in Paper 3 were based on information from existing literature of previous earthquakes in other geographic areas with corresponding magnitudes and faulting mechanism, occurring in similar tectonic settings. Uncertainty in the input parameters introduces uncertainties in the simulations. As concluded in section 3.3 and in Paper 3, the worst case scenario in terms of seismic hazard for İzmir was found to be a rupture along the İzmir fault. Hence, the effect of varying the input parameters in the ground motion simulations was tested for a rupture along this fault.

Previously, such tests have been conducted for the Marmara Sea segment of the North Anatolian fault (Pulido et al., 2004; Sørensen et al., 2007b). In the present study, the scenario earthquake had a smaller magnitude and a different faulting mechanism (normal fault versus strike-slip fault) and tests of more input parameters were included.

The method for this study followed the approach of Pulido et al. (2004) and Sørensen et al. (2007b), where a reference scenario was defined and source and regional crustal parameters were changed one by one in a total of 27 test scenarios. The tested parameters included fault depth, attenuation (in terms of frequency dependent Q), rupture initiation point, velocity model, seismic moment, stress-drop ratio (ratio between background and asperity stress-drop), average stress-drop, rise time, rupture velocity, dip, rake and asperity location (for details on the reference scenario and the tested parameters see Table 1 in Paper 4). The ground motions were calculated for bedrock conditions, and the effect of the sediment deposits underlying İzmir were not considered in this study. The problem of site effects is treated in section 3.5 and Paper 5.

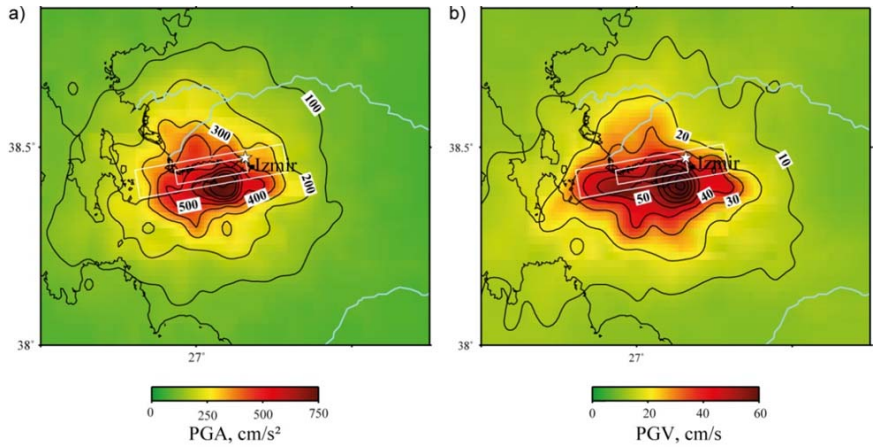

Figure 14. PGA and PGV distributions for the reference scenario. White lines show the surface projection of the fault plane and asperity, and the white star indicates the epicenter.

The distribution of PGA and PGV from the reference scenario is shown in Figure 14. The obtained simulated ground motion levels were higher than what was observed from the earthquake scenario along İzmir fault in Paper 3. For the parameter sensitivity study a simpler fault model was assumed. The fault was assumed to consist of a single segment, rather than three segments as assumed in Paper 3. The fault width was slightly changed, and only one asperity was assumed, whereas there were two in the study of Paper 3. The asperity in the parameter sensitivity study was also located closer to the surface. Comparing the simulated ground motions from the two scenarios with empirical attenuation relations shows that the reference scenario in Paper 4 fits the empirical relations better than the simulations from the scenario earthquake 1C IF along İzmir fault in Paper 3 (Figure 15).

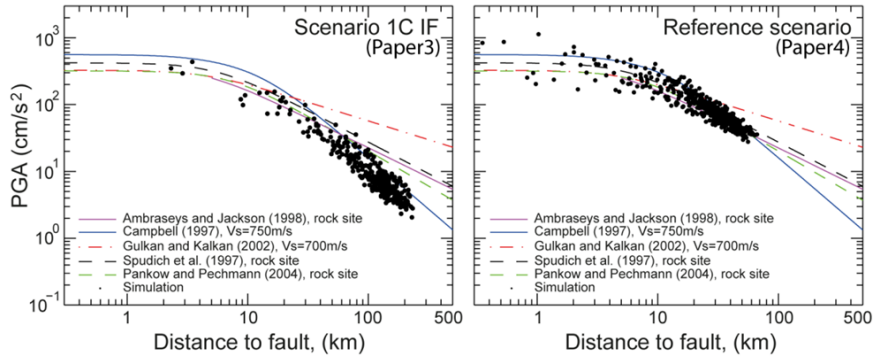

Figure 15. Comparison of the simulated peak ground accelerations to empirical attenuation relations, see labels for details. Scenario 1C IF in Paper 3 (left) and the reference in Paper 4 (right).

The simulated ground motion distributions from the test scenarios were compared to the distribution of the ground motions obtained from the reference scenario. The parameters that were found to influence the ground motion most in terms of absolute change in ground shaking level were the applied velocity model, seismic moment, rise time and rupture velocity. In addition, stress-drop and attenuation model control the change in absolute ground motion level to a large extent, if these parameters were changed sufficiently.

The largest variability of ground motion was observed above the fault. This is shown as the distribution of the standard deviation of PGA and PGV of the reference scenario and the 27 test scenarios in Figure 16. The largest variability is found directly above the surface rupture of the fault plane, corresponding to the most central part of İzmir. Close to the asperity and rupture initiation point the standard deviation is found to exceed 200 cm/s^2 and 20 cm/s for PGA and PGV, respectively. For larger distances the variation of the simulated ground motions decreases.

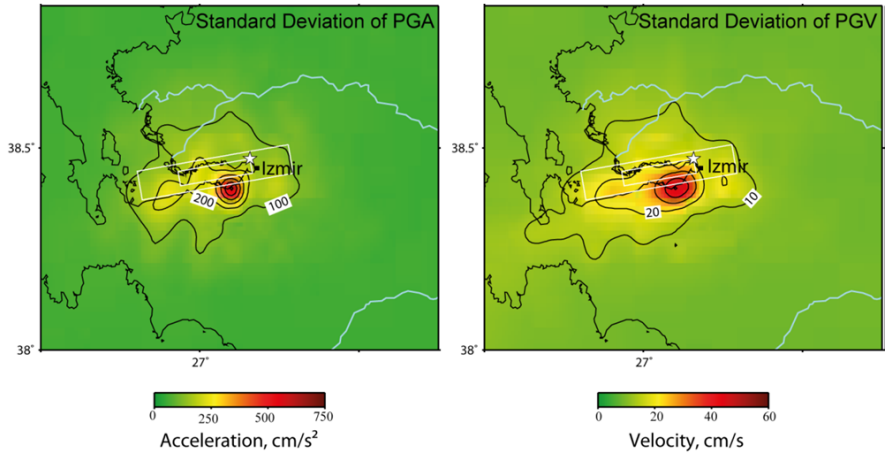

Figure 16. Spatial distribution of standard deviation of PGA (left) and PGV (right) based on the reference scenario and the 27 test scenarios. Surface projection of the fault plane and asperity of the reference scenario are shown as white boxes; the rupture initiation point of the reference scenario is indicated as a star.

The input parameters were found to affect the simulated ground motions in different frequency bands. Stress-drop, stress-drop ratio and Q only affected the high-frequency ground motions, while location of rupture initiation, seismic moment, fault depth, rise time and velocity model had the largest effect on the low-frequency ground motions.

The 5% damped velocity response spectra for a site in the center of İzmir, for the reference scenario and the 27 test scenarios is shown in Figure 17. A large variation among the different scenarios was found and the spectral level of the reference scenario represents an average. For the lower frequencies, larger variation among the different scenarios was observed, than for the higher frequencies. This is also illustrated in Figure 18 of Paper 4, where the distribution of the standard deviation of the response spectral velocity is shown in three frequency bands.

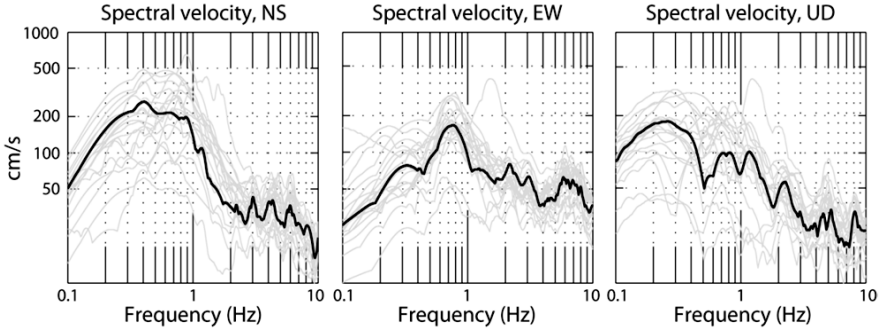

Figure 17. 5% damped spectral velocity for a station located in the center of İzmir. The black line show the spectral velocity for the reference scenario, while the gray lines are for the 27 test scenarios.

This study showed the importance of considering several earthquake scenarios, when assessing the seismic hazard through ground motion simulations. With this approach the variability of ground motions from several scenarios are considered in the hazard assessment. For İzmir it was found that the most populated area along the coast of İzmir Bay, coincide with the area where the largest variability in ground motion for an earthquake rupture along İzmir fault is predicted. This suggests a challenge in the structural engineering of buildings and structures in the area.

3.5 Estimation of ground motions taking into account soil conditions

The city of İzmir is largely located on sediment deposits, and seismic waves are expected to amplify as they propagate through the soil layer overlying the bedrock. Until now the ground motions presented for İzmir have been calculated for bedrock conditions, and local site effects are therefore not included. In Paper 5 the local site effects are considered in order to provide a more reliable hazard estimate. This exercise is done for selected sites in İzmir.

Even without an earthquake, soft soil conditions for various sites in İzmir are a problem. Figure 18 shows pictures of buildings in the Karşıyaka district of İzmir, which are sinking into the ground and tilting due to the soft soil foundation. The ages of the houses are up to 20 years, and these structures have therefore not experienced strong ground shaking due to a large earthquake. Site effects during an earthquake are of high importance when considering the seismic hazard in İzmir.

Figure 18. Pictures of houses in the Karşıyaka, district of İzmir. Tilting of the structures due to soft soil conditions is visible. The picture at the lower right is from the rear of the house shown in the upper row. The angle between the yellow lines is approximately 10-15°.

In the İzmir Earthquake Master Plan the problem of local site effects for İzmir was treated and presented as maps of expected amplification and liquefaction potential (Figure 19) (MMI, 2000). The amplification potential was estimated through core penetration tests. From this, large amplifications were expected for the northern side of İzmir Bay, as well as in the center of the city (innermost part of the bay). Furthermore, it is clear that liquefaction during strong ground shaking is an important issue to consider.

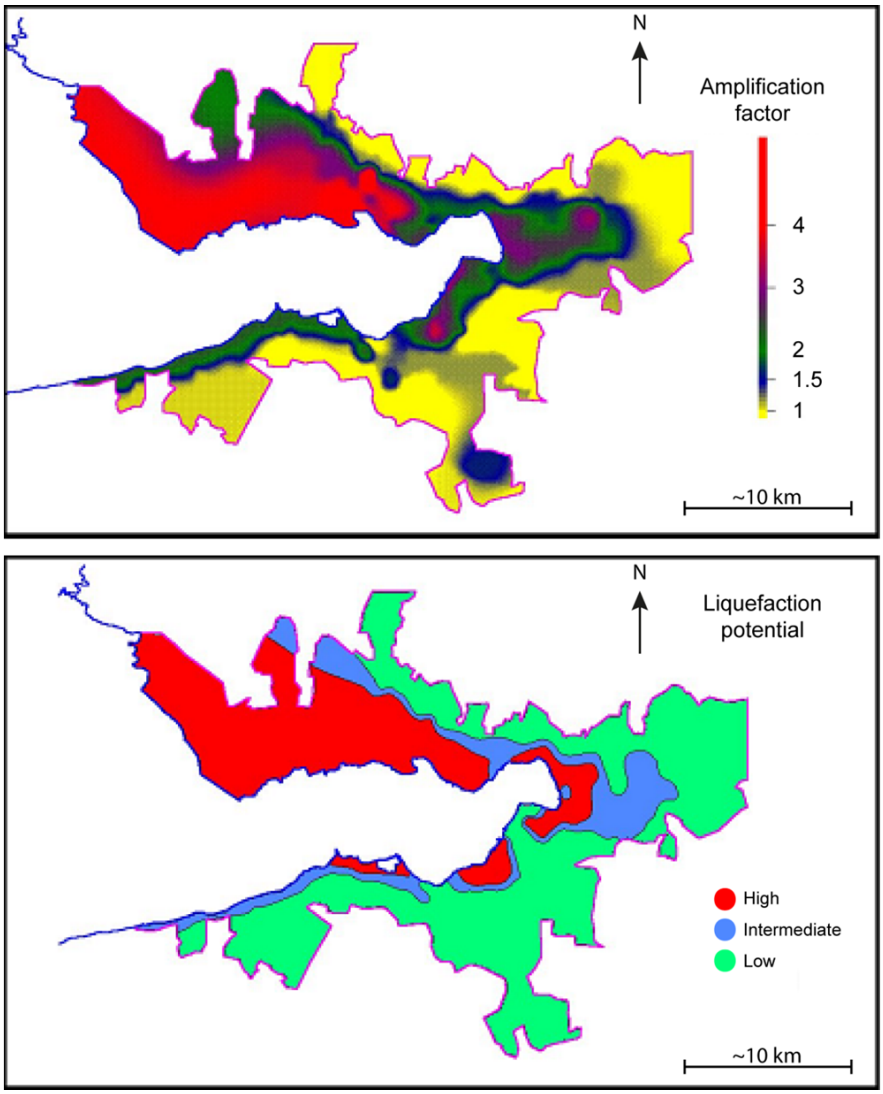

Figure 19. Amplification factors (top) and liquefaction potential (bottom). The colored area corresponds to the limits of the metropolitan area of İzmir. Modified from MMI. (2000).

The study by MMI (2000) does not consider the frequency dependency of the amplification, which is necessary in order to determine the change in frequency content of the seismic waves from bedrock level to the top of a soil column. In Paper 5 this problem was treated using H/V spectral ratios (Lermo and Chávez-García, 1994; Nakamura, 1989; 2008; 2010) obtained from ambient noise measurements as transfer functions. The ground motions simulated for bedrock

conditions are convolved with transfer functions in order to estimate the ground motion on top of the soil columns (Kramer, 1996). In this study the reference scenario of Paper 4 was used as input ground motion. The variation of the ground motion due to input parameter uncertainty was not considered in this study.

Soil conditions vary across İzmir, where topographic high areas are associated with bedrock outcrops, while topographic low areas are located on sediment deposits. Due to several rivers emptying into İzmir Bay, the thickness of the sediment layers is expected to vary, although no detailed information concerning this is available. The Gediz River used to have its mouth on the northern coast of İzmir Bay, close to the Mavişehir district (see Figure 20 for locations). The river is now redirected, but the old river delta, located in Mavişehir, is expected to consist of very thick sedimentary deposits. In the inner part of İzmir Bay, Kavak River plays a role. This river is not as large as the Gediz River, and it is therefore thought to transport less fluvial deposits. The thickness of the sediments in this area is therefore considered to be less than in the western part of the bay.

Ambient noise measurements were conducted across most of İzmir in a 2 by 2 km grid. Focus was given to three areas within the city, where detailed measurements were taken within a small area. This was done for Karşıyaka, Konak and Mavişehir (see Figure 20 for locations). From the H/V spectral ratios, information on fundamental frequency and amplification was extracted. General agreement exists on the method's ability to estimate the fundamental frequency, while the capability of the method to predict the amplification is under debate (Bour et al., 1998; Huang et al., 2002; Nakamura, 1989; 2010; Teves-Costa et al., 1996). Comparing the distribution of expected amplification in Figure 20 with the amplification factors from MMI (2000), the distribution of higher and lower expected amplification fits well, although the two studies do not always agree on the level of amplification. Compared to the study by MMI (2000) the expected amplification from the H/V spectral ratios did not systematically over- or underestimate the previous values. Despite the uncertainty in the estimated amplification, it was found appropriate to use the amplification values from the H/V spectral ratios in the transfer functions in an initial attempt to estimate ground motions taking into account soil conditions within İzmir. For the areas Karşıyaka, Konak and Mavişehir average H/V spectral ratios were calculated based on the measurements in each of these areas. The ground motion corrected for soil conditions was calculated and higher ground motion levels were found, see Table 4 of Paper 5 for details.

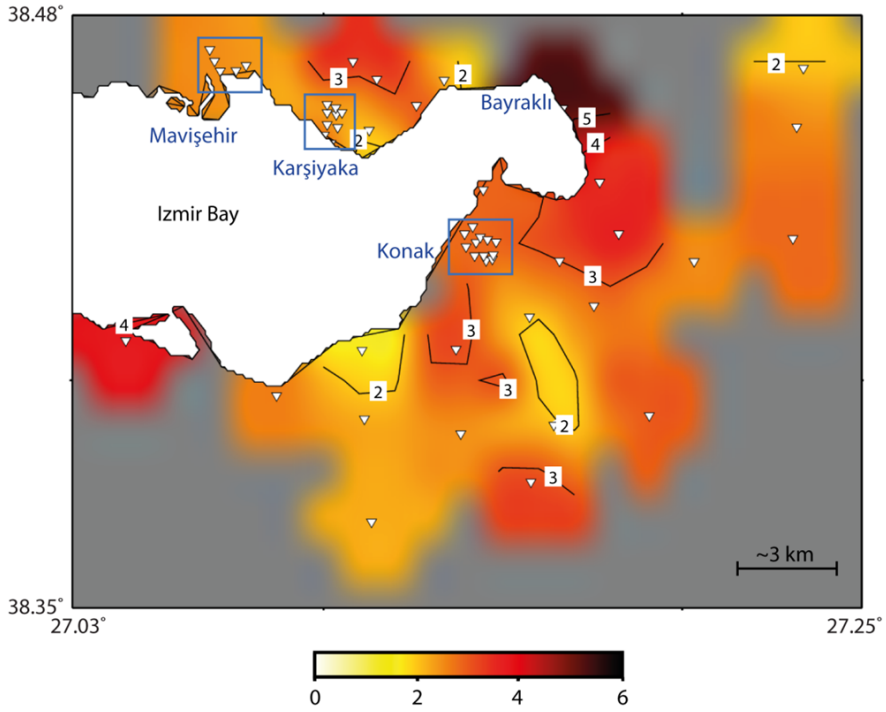

Figure 20. Distribution of maximum amplification factor found from the H/V spectral ratios. The sites of special interest are marked with blue boxes. Triangles show the locations of measurements.

Nakamura (2010) uses a value, *Kg* ($Kg = A^2/f_0$, where A is the amplification and f_0 is the fundamental frequency), to estimate ground failure potential, such as liquefaction, during large bedrock ground shaking. The *Kg* value found based on the H/V spectral ratio confirmed ground failure potential, such as liquefaction, in the area around Bayraklı (innermost part of the bay to the north) for bedrock ground motions lower than what was found from the ground motion simulation. Using the amplification factors from Erdik et al. (2000) in the calculations for Kg, the areas of Mavişehir and Karşıyaka were also found to be potential locations for ground failure during an earthquake rupture along İzmir fault. This is consistent with the high water level in the area, as well as sinking of the structures into the top-most soil layer, especially in Karşıyaka (Ziya Çakir, personal communication).

For the area of Karşıyaka initial estimates of the soil column were modeled, by calculating the theoretical soil response, and comparing this to the H/V spectral ratio obtained from field measurements of ambient noise. This was done even though very limited knowledge on the soil structure for the area exists and with no borehole data or seismic reflection surveys to constrain the thickness of the

soil column. The modeling of transfer functions was conducted using SHAKE2000 (Ordóñez, 2011). The soil response of a soil column was calculated and the fundamental frequency of the obtained transfer function was matched to the fundamental frequency found from the H/V spectral ratio for Karşıyaka. Two soil columns of different thickness (60 m and 100 m) were modeled, using the relation between fundamental frequency, f_0 , average shear wave velocity, $v_{s,ave}$, and thickness of soil column, H:

$$f_0 = \frac{v_{s,ave}}{4 \cdot H} \ .$$

The modeling was done by a trial-and-error approach.

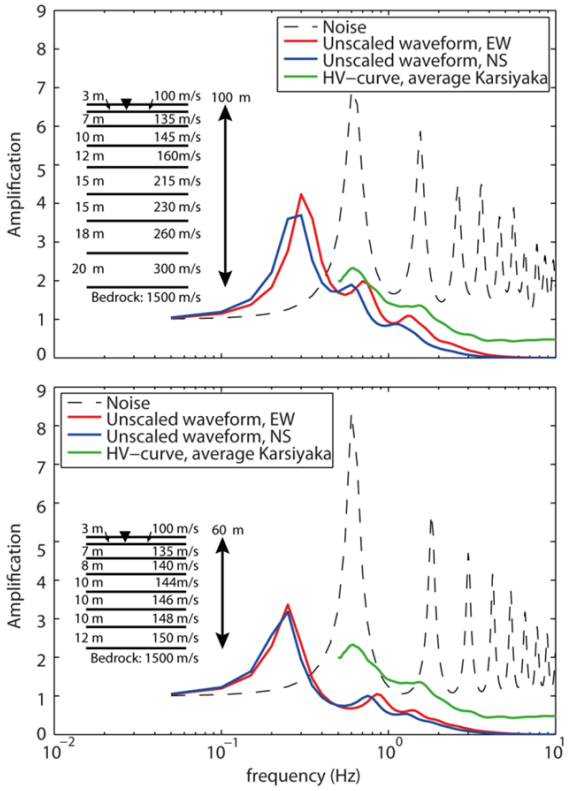

Figure 21. Transfer functions calculated for the two soil columns. The type of input ground motion is given in the legend, and the average H/V-curve for Karşıyaka is shown in green. The modeled soil columns are also shown with corresponding layer thicknesses and velocities.

In Figure 21 the transfer functions obtained when propagating ambient noise and the simulated waveform through the obtained soil columns are shown. The

transfer functions obtained when ambient noise is propagated through the soil column predict much larger amplification than found from the H/V spectral ratio. Also, when larger ground motions are used as input, the strain is large and the fundamental frequency and amplification decreases, as expected from the relation between shear wave velocity and frequency in the equation above, together with the relation between shear modulus/rigidity, G, and shear wave velocity

$$v_s = \sqrt{\frac{G}{\rho}},$$

where ρ is the density. The largest amplification of bedrock ground motion, due to the soil response of the two soil columns is found for the soil column of 100 m thickness.

The study verified that local site effects across İzmir are an important issue in hazard assessment for İzmir. The study in Paper 5 is meant as an preliminary study for identifying site effect potential and soil structures within the city of İzmir. The study is based on several assumptions and simplifications. It should be extended with focus on obtaining velocity structures of the soil columns. With such an approach the soil response due to large bedrock ground motions can be treated with a non-linear approximation.

4. Conclusions

Two case studies have been presented in this thesis. A kinematic hybrid broadband frequency ground motion simulation technique has been applied, in order to study the seismic hazard near Wenchuan, China and İzmir, Turkey. The following conclusions can be drawn based on this work:

For Wenchuan, China:

- The ground motion simulations of the May 12, 2008 Wenchuan, China earthquake reproduce to a large extent the observed ground motion. The simulated peak ground motion correlates with the observed ground motion levels, although topography and local site effects have not been considered in the simulations.
- The width of the fault plane in the input model used in the simulations of the Wenchuan earthquake affects the simulation results significantly due to the influence on the stress-drop. The simulated ground motions match the observations best when the input model is 40 km wide.
- The predominant periods of the simulated ground motions coincide with those observed, and with the fundamental periods of many of the buildings in the earthquake affected area of the Wenchuan earthquake. The extensive damage observed is explained by this, along with the shear size of the earthquake and poor construction practices, especially for the older buildings.
- The strong ground shaking, mountainous landscape, extensive landslides and rock falls have exacerbated the human and economic consequences of the affected area. Fault rupture complexities further contributed to the intensity and distribution of the damage, with a rupture directivity enhancing the ground motions along the fault, as clearly demonstrated e.g.

in Beichuan, located on the surface rupture of the fault in the forward rupture directivity direction.

For İzmir, Turkey:

- The worst case scenario in terms of seismic hazard in İzmir is a rupture of the entire 42 km long İzmir fault, corresponding to an M_w 6.9 earthquake, striking underneath the city. The attenuation of the simulated ground motions away from the fault is found to agree well with empirical attenuation relations, which indicates realistic rupture scenarios. Ground shaking on bedrock level, for the central part of the city, is expected to exceed 750 cm/s^2 and 60 cm/s for PGA and PGV, respectively.

- The input parameters with the largest influence on the absolute ground motion level are the velocity model, the seismic moment, rise time and rupture velocity. Stress-drop and attenuation will influence the absolute level of ground motion significantly, if they are sufficiently changed.

- The largest variability in the simulated ground motion is found above the fault plane with standard deviations exceeding 200 cm/s^2 and 20 cm/s for PGA and PGV, respectively.

- The low-frequency ground motion is mostly affected by the location of rupture initiation, seismic moment, fault depth, rise time and rupture velocity. These parameters are therefore the most important when it comes to building damage potential. The attenuation model, average stress-drop and stress-drop ratio only affect the high-frequency ground motion.

- The fundamental frequencies found from H/V spectral ratios correlate well with the topographic changes within İzmir. Low lying coastal areas, located on sedimentary deposits, are associated with very low fundamental frequencies, while topographic high areas, associated with bedrock outcrops, are found to have higher fundamental frequencies.

- The amplification factors found from the H/V spectral ratios are in fairly good agreement with previous estimates. Large amplification of seismic waves is expected in the innermost and northern part of İzmir Bay. Based on Kg values, especially Bayraklı is suggested to have significant soil

deformation potential, such as liquefaction, during an earthquake rupture along İzmir fault.

- The ground motions taking into account soil conditions, calculated from the H/V spectral ratios obtained from field measurements, are found to be amplified when compared to the ground motions for the bedrock conditions.
- The soil response of two modeled soil columns for Karşıyaka imply an increase in ground motions on top of the soil layer for the lower frequencies, compared to the bedrock ground motion. The thicker model of 100 m results in the largest amplification level of the ground motion.

The hybrid broadband simulation technique was found to be a powerful tool to simulate realistic ground motions. The simulated ground motions are comparable to observed values in retrospect studies, as long as realistic input models are used. Comparing the performance of the applied simulation technique in the two case studies presented in this thesis and with previous studies of the M_w 6.8, 2000 Tottori, Japan (Pulido and Kubo, 2004) and the M_w 9.3, 2004 Sumatra, Indonesia (Sørensen et al., 2007a) earthquakes, the method is found to successfully simulate earthquakes over a range of magnitudes. Based on this, the simulation method is found appropriate to obtain realistic ground motion estimates where the seismic hazard assessments are deficient due to very large return periods. Occurrence of earthquakes as the 2008 Wenchuan, China and the 2011 Honshu, Japan earthquakes confirms that exercises of simulating ground motions, even for events expected to have extremely low occurrence probability, are important in seismic hazard assessments. Nevertheless, it is important to keep in mind that the ground motion simulations do not assign a probability of the occurrence of the simulated scenarios. The probability of occurrence, together with the expected ground shaking level and dominating frequencies obtained from the simulations, is important information for city planners and engineers when determining the level of conservatism to be applied in the design of buildings and structures.

The comparison of the different ground motion simulation studies of the Wenchuan earthquake, presented in the special issue on the earthquake in Bulletin of the Seismological Society of America, showed that the different kinematic simulation methods to a large extent are capable of reproducing the observed ground motion level and the frequency content of the seismic waves,

while exact representations of the seismograms are more difficult to reproduce. In that sense, the hybrid broadband frequency simulation technique applied in this thesis performs equally well as the other simulation techniques.

When applying deterministic ground motion simulations in seismic hazard assessments it is important to keep in mind that the uncertainty in the input parameters are known to have a large effect on the simulated ground motions. Several earthquake scenarios, with varying rupture parameters, must therefore be considered when the seismic hazard for an area is assessed through ground motion simulations. The variation found in the simulated ground motion due to input parameter uncertainty is expected to be representative for similar exercises using other ground motion simulation techniques than the technique applied in this study.

5. Future perspectives

Assessment of seismic hazard is a continuing process, and the input models used in the calculations of ground motion, as shown in this thesis, can always be improved. The problem of uncertainties in input parameters (Section 3.4 and Paper 4) can be addressed through more detailed studies of the faults in question. Investigation of the input parameters and fault geometry, including asperity location, can hopefully lower the level of uncertainty in the simulated ground motions. Also, inclusion of the site effect potential should be incorporated in the simulations, either by the use of EGF or by site effect potential estimates for the area of interest, as described in Section 3.5 and Paper 5. Specific suggestions for future work regarding the seismic hazard assessment of both the Wenchuan area and İzmir are given in the following sections.

5.1 Future aspects in assessing the seismic hazard for the Wenchuan area

Following the 2008 Wenchuan earthquake, Coulomb stress transfer analysis have been conducted (e.g. Parsons et al., 2008; Toda et al., 2008). These studies yield increased stresses on several faults in the area close to the fault rupture of the Wenchuan earthquake. According to Parsons et al. (2008) the largest stress increase were identified for the Xianshuihe fault (see Figure 1 for location). This is a left-lateral strike-slip fault, with Coulomb stress increase over a length of more than 125 km. Such a rupture length corresponds to an earthquake of magnitude 7.5 (Wells and Coppersmith, 1994). Similar Kunlun fault (right-lateral strike slip fault) is brought closer to rupture, which is a fault of almost 200 km length. Both of these faults are known to have produced earthquakes of $M > 7$ in the past, and pose a significant threat to the area along the faults. Therefore, ground motion simulations of these scenario earthquakes should be conducted in order to estimate expected ground shaking in the areas of these faults, and attempts to mitigate the seismic risk, e.g. by building reinforcement should be initiated.

The 2008 Wenchuan earthquake occurred in an area of high site effect potential. Topographic high peaks and deep valleys with sedimentary fill of varying depths add to a very complex picture. The site effect potential should be investigated in detail, and included in the simulations for a better understanding of the ground motion distribution. The input models used in the ground motion simulations (Section 2.1 and Paper 1) can be refined to better match the recorded waveforms of the 2008 Wenchuan earthquake when they become available to the scientific community. This concerns e.g. asperity location and variation of the rupture velocity on the different fault segments, corresponding to higher rupture velocity on the northern segment, which ruptured with strike-slip mechanism, compared to the southern segment, rupturing with a thrust mechanism.

The heavily damaged area following the 2008 Wenchuan earthquake will take a long time to re-build. In some of the visited cities during the field trip in October 2008, *"earthquake memorial parks"* were planned as memorials and museums for structural engineers to study types of building damage. This will hopefully contribute to improved knowledge and building practices in areas with potential to experience strong ground shaking due to earthquakes.

5.2 Future actions needed in the hazard assessment of İzmir

Assessing the seismic hazard through scenario based deterministic methods is appropriate to apply in areas where the seismic hazard is controlled by single nearby faults. However, in such a case the earthquake recurrence and its statistical basis are not recognized. On the other hand, the standard probabilistic approach ignores fault interaction, stress transfer and fault rupture complexity due to the fault rupture dynamics and wave propagation. Therefore, in cases, like İzmir, where several active faults exist, having the potential of generating destructive earthquakes, the seismic hazard must be treated through methodologies which link the scenario based on deterministic ground motion simulations with probabilistic seismic hazard assessment.

The earthquake history of İzmir, with three large earthquakes in a period of 90 years followed by a long period of quiescence, indicates fault linkage. Attention should therefore be given to investigating this problem, and stress transfer analyses should be conducted for different fault rupture scenarios along the faults in the area.

As the results presented in Section 3.3 and in Paper 3 also identified a rupture along Tuzla fault to pose a threat towards İzmir, analyses of the ground motion variability due to parameter uncertainty should be considered for such a scenario earthquake. However, there are many faults in the area together with many population centers and therefore, detailed studies for several rupture scenarios are important to assess the seismic hazard in the area.

On the northern side of the İzmir Bay, Cigli fault crosses the area through Karşıyaka and the ancient part of İzmir. The fault was classified as a non-active fault by Emre et al. (2005). However, evidence of this fault extending offshore in the outer İzmir Bay and with small earthquakes offshore, imply possible activity along this. A rupture along this fault, as a rupture along İzmir fault, will have serious consequences for İzmir. The potential ground shaking from such a scenario earthquake should be investigated.

A preliminary study of the site effect potential for the selected sites within İzmir was presented in Section 3.5 and Paper 5. This work must be continued and expanded. A technique based on array measurements of ambient noise is suggested for obtaining the seismic velocity structure through dispersion curve inversion. Information on the soil properties is needed in order to treat the problem of site amplification in a non-linear way, which is needed since large bedrock ground motions are expected during a future earthquake along İzmir fault.

Data and Resources

Many of the figures in this text and in the research papers were made using Generic Mapping Tools (GMT) (Smith and Wessel, 1990; Wessel and Smith, 1998).

The ground motion simulations were calculated with BroadBand Simulation (BBSIM) program package version 1.2 (Nelson Pulido, personal communication).

In the study presented in Section 3.5 and Paper 5, SEISLOG (Utheim and Havskov, 1998) was used for data acquisition and SEISAN (Ottemöller et al., 2011) was used for checking and organizing the data. The ambient noise data was processed using GEOPSY (Wathlet, 2011). SHAKE2000 (Ordóñez, 2011) was used in the modeling of transfer functions.

References

Aki, K., Richards, P.G. (2002). Quantitative seismology. University Science Books, Sausalito, California, 700p.

Aktuğ, B.,Kılıçoğlu, A. (2006). Recent crustal deformation of İzmir, western Anatolia and surrounding regions as deduced from repeated GPS measurements and strain field. Journal of Geodynamics, v.41(5), pp.471-484.

Ambraseys, N.N., Finkel, C.F. (1995). The seismicity of Turkey and adjacent areas, a historical review, 1500-1800. Muhittin Salih EREN, Istanbul, 240p.

Ambraseys, N.N., Jackson, J.A. (1998). Faulting associated with historical and recent earthquakes in the Eastern Mediterranean region. Geophysical Journal International, v.133(2), pp.390-406.

Archuleta, R.J., Day, S.M. (1980). Dynamic rupture in a layered medium: the 1966 Parkfield earthquake. Bulletin of the Seismological Society of America, v.70(3), pp.671-689.

Archuleta, R.J., Frazier, G.A. (1978). Three-dimensional numerical simulations of dynamic faulting in a half-space. Bulletin of the Seismological Society of America, v.68(3), pp.541-572.

Benetatos, C., Kiratzi, A., Ganas, A., Ziazia, M., Plessa, A., Drakatos, G. (2006). Strike-slip motions in the Gulf of Sigacik (western Turkey), Properties of the 17 October 2005 earthquake seismic sequence. Tectonophysics, v.426(3-4), pp.263-279.

Beresnev, I.A., Atkinson, G.M. (1997). Modeling finite-fault radiation from the ω^n spectrum. Bulletin of the Seismological Society of America, v.87(1), pp.67-84.

Beresnev, I.A., Atkinson, G.M. (1998). Stochastic finite-fault modeling of ground motions from the 1994 Northridge, California, earthquake. I. Validation on

rock sites. Bulletin of the Seismological Society of America, v.88(6), pp.1,392-1,401.

Bird, P. (2003). An updated digital model of plate boundaries. Geochemistry Geophysics Geosystems, v.4(3), pp. 1,027-1,052.

Boore, D.M. (1983). Stochastic simulation of low-frequency ground motions based on seismological models of the radiated spectra. Bulletin of the Seismological Society of America, v.73(6A), pp.1,865-1,894.

Boore, D.M. (2003). Simulation of ground motion using the stochastic method. Pure and Applied Geophysics, v.160(3-4), pp.635-676.

Boore, D.M., Boatwright, J. (1984). Average body-wave radiation coefficients. Bulletin of the Seismological Society of America, v.74(5), pp.1,615–1,621.

Bouchon, M. (1981). A simple method to calculate Green's functions for elastic layered media. Bulletin of the Seismological Society of America. v.71(4), pp.959-971.

Bour, M., Fouissac, D., Dominique, P., Martin, C. (1998). On the use of microtremor recordings in seismic microzonation. Soil Dynamics and Earthquake Engineering, v.17(7-8), pp.465-474.

Brune, J.N. (1970). Tectonic stress and the spectra of seismic shear waves from earthquakes. Journal of Geophysical Research, v.75(26), pp.4,997-5,009.

Burchfiel, B.C., Royden, L.H., Hilst, R.D.v.d, Hager, B.H., Chen, Z., King, R.W., Li, C., Lü, J., Yao, H., Kirby, E. (2008). A geological and geophysical context for the Wenchuan earthquake of 12 May 2008, Sichuan, People's Republic of China. GSA Today, v.18(7), pp.4-11.

Campbell, K.W. (1997). Empirical near-source attenuation relationships for horizontal and vertical components of peak ground acceleration, peak ground velocity, and pseudo-absolute acceleration response spectra. Seismological Research Letters, v.68(1), pp.154-179.

Chavez, M., Cabrera, E., Madariaga, R., Chen., H, Perea, N., Emerson, D., Slazar, A., Ashworth, M., Moulinec, Ch., Li, X., Wu, M., Zhao, G. (2010). Low-frequency 3D wave propagation modeling of the 12 May 2008 Mw 7.9 Wenchuan Earthquake. Bulletin of the Seismological Society of America, v.100(5B), pp.2,561-2,573.

Chen, Z., Burchfiel, B.C., Liu, Y., King, R.W., Royden, L.H., Tang, W., Wang, E., Zhao, J., Zhang, X. (2000). Global Positioning System measurements from eastern Tibet and their implications for India/Eurasia intercontinental deformation. Journal of Geophysical Research, v.105(B7), pp.16,215-16,227.

DeMets, C., Gordon, R.G., Argus, D.F., Stein, S. (1990). Current plate motions. Geophysical Journal International, v.101(2), pp.425-478.

Deniz, A., Korkmaz, K.A., Irfanoglu, A. (2010). Probabilistic seismic hazard assessment for İzmir, Turkey. Pure and Applied Geophysics, v.167(12), pp.1,475-1,484.

Emre, Ö., Özalp, S., Dogan, A., Özaksoy, V., Yildirim, C., Göktas, F. (2005). Active faults in the vicinity of İzmir and their earthquake potential (in Turkish). Report No. 10754, Geological Studies Department, General Directorate of Mineral Research and Exploration, Ankara, Turkey.

Ghasemi, H., Fukushima, Y., Koketsu, K., Miyake, H., Wang, Z., Anderson J.G. (2010). Ground-motion simulation for the 2008 Wenchuan, China, earthquake using the stochastic finite-fault model. Bulletin of the Seismological Society of America, v. 100(5B), pp.2,476-2,490.

Giardini, D., Gupta, H., Giesecke, A., Dimaté, C., Shedlock, K., Grunthal, G., Garcia, M., Iben Brahim, B., Slejko, D., Musson, R., Balassanian, S., Ulomov, V., Ashtiany, M.G., Atakan, A., Nyambok, I., Zhang, P., McCue, K., Engdahl, E., McGuire, R., Mayer-Rose, D. (1999). Global Seismic Hazard Assessment Program. http://www.seismo.ethz.ch/GSHAP/. Last accessed April 2011.

Gülkan, P., Kalkan, E. (2002). Attenuation modeling of recent earthquakes in Turkey. Journal of Seismology, v.6(3), pp.397-409.

Harris, R.A. (2004). Numerical simulations of large earthquakes: Dynamic rupture propagation on heterogeneous faults. Pure and Applied Geophysics, v.161(11-12), pp.2,171-2181.

Hartzell, S.H. (1978). Earthquake aftershocks as Green's functions. Geophysical Research Letters, v.5(1), pp.1-4.

Hartzell, S., Harmsen, S., Frankel, A., Larsen, S. (1999). Calculation of broadband time histories of ground motion: Comparison of methods and validation using strong-ground motion from the 1994 Northridge earthquake. Bulletin of the Seismological Society of America, v.89(6), pp.1,484-1,504.

Hartzell, S., Guatteri, M., Mai, M.P., Liu, P.-C., Fisk, M. (2005). Calculation of broadband time histories of ground motion, part II: Kinematic and dynamic modeling using theoretical Green's functions and comparison with the 1994 Northridge earthquake. Bulletin of the Seismological Society of America, v.95(2), pp.614-645.

Huang, H.-C., Yang, Y.-T., Chiu, H.-C. (2002). Site response evaluation using H/V ratio at the Yan-Liau station in Hualien, Taiwan. Pure Applied Geophysics, v.159(11-12), pp.2,715-2,731.

Hubbard, J., Shaw, J.H. (2009). Uplift of the Longmen Shan and Tibetan plateau, and the 2008 Wenchuan (M=7.9) earthquake. Nature, v.458(7535), pp.194-197.

Irikura, K. (1986). Prediction of strong acceleration motion using empirical Green's functions. Proceedings 7th Japan Earthquake Symposium, Japan, pp.151-156.

Iwata, T., Irikura, K. (1988). Source parameters of the 1983 Japan-Sea earthquake sequence. Journal of Physics of the Earth, v.36(4), pp.155-184.

Jimenez, M.-J., Giardini, D., and Grunthal, G., (2003). The ESC-SESAME Unified Hazard Model for the European-Mediterranean region. EMSC/CSEM Newsletter, v.19, pp.2-4.

Jolivet, L. (2001). A comparison of geodetic and finite strain pattern in the Aegean, geodynamic implications. Earth and Planetary Science Letters, v.187(1-2), pp.95-104.

Ji, C., Hayes, G. (2008). Source model of the May 12th 2008 Wenchuan earthquake. http://earthquake.usgs.gov/eqcenter/eqarchives/poster/2008/20080512.php. Last accessed May 2009.

Kamae, K., Irikura, K., Pitarka, A. (1998). A technique for simulating strong ground motion using hybrid Green's function. Bulletin of the Seismological Society of America, v.88(2), pp.357-367.

Klinger, C., Ji, C., Shen, Z.-K., Bakun, W.H. (2010). Introduction to the special issue on the 2008 Wenchuan, China, earthquake. Bulletin of the Seismological Society of America, v.100(5B), pp.2,353-2,356.

Koketsu, K., Hikima, K., Miyake, H., Maruyama, T., Wang, Z. (2008). Source process and ground motions of the 2008 Wenchuan, China, earthquake. Abstract S31B-1914, EOS Trans. AGU, v.89(53) Fall Meeting Supplement.

Koketsu, K., Yokota, Y., Ghasemi, H., Hikima, K., Miyake, H., Wang, Z. (2009). Source process and ground motions of the 2008 Wenchuan earthquake, Investigation report of the May 12th 2008, Wenchuan earthquake, China. Grant-in-Aid for Special Purposes of 2008, Ministry of Education, Culture, Sports, Science and Technology (MEXT), No. 20900002.

Kramer, S.L. (1996). Geotechnical earthquake engineering. Prentice Hall, Upper Saddle River, New Jersey, 653 p.

Kurahashi, S., Irikura, K. (2010). Characterized source model for simulating strong ground motions during the 2008 Wenchuan earthquake. Bulletin of the Seismological Society of America, v.100(5B), pp.2,450-2,475.

Lermo, J., Chávez-García, F.J. (1994). Are microtremors useful in site response evaluation? Bulletin of the Seismological Society of America, v.84(5), pp.1,350-1,364.

Li, X., Zhou, Z., Huang, M., Wen, R., Yu, H., Lu, D., Zhou, Y., Cui, J. (2008a). Preliminary analysis of strong-motion recordings from the magnitude 8.0 Wenchuan, China, Earthquake of 12 May 2008. Seismological Research Letters, v.79(6), pp.844-854.

Li, X., Zhou, Z., Yu, H., Wen, R., Lu, D., Huang, M., Zhou, Y., Cui, J. (2008b). Strong motion observations and recordings from the great Wenchuan Earthquake. Earthquake Engineering and Engineering Vibrations, v.7(3), pp.235-246.

Lin, A., Ren, Z., Jia, D., Wu, X. (2009). Co-seismic thrusting rupture and slip distribution produced by the 2008 Mw 7.9 Wenchuan earthquake, China. Tectonophysics, v.471(3-4), pp.203-215.

Liu, P., Archuleta, R.J., Hartzell, S.H. (2006). Prediction of broadband ground-motion time histories: Hybrid low/high-frequency method with correlated random source parameters. Bulletin of the Seismological Society of America, v.96(6), pp.2,118-2,130.

Madariaga, R. (1976). Dynamics of an expanding circular fault. Bulletin of the Seismological Society of America, v.67(3), pp.163-182.

Madriaga, R. (1989). Seismic source: Theory. In: The encyclopedia of soild earth geophysics. Editor: David E. James, Van Nostrand Reinhold Company, New York, pp.1,129-1,133.

McClusky, S., Balassanian, S., Barka, A., Demir, C., Ergintav, S., Georgiev, I., Gurkan, O., Hamburger, M., Hurst, K., Kahle, H., Kastens, K., Kekelidze, G., King, R., Kotzev, V., Lenk, O., Mahmoud, S., Mishin, A., Nadariya, M., Ouzounis, A., Paradissis, D., Peter, Y., Prilepin, M., Reilinger, R., Sanli, I., Seeger, H., Tealeb, A., Toksöz, M.N., Veis, G. (2000). Global Positioning System constraints on plate kinematics and dynamics in the eastern Mediterranean and Caucasus. Journal of Geophysical Research, v.105(B3), pp.5,695-5,719.

Metropolitan Municipality of İzmir (MMI) (2000). İzmir earthquake master plan (in Turkish). http://www.İzmir.bel.tr/İzmirdeprem/İzmirrapor.htm, Metropolitan Municipality of İzmir publication, İzmir, Turkey. Last Accessed March 2011.

Nakamura, Y. (1989). A method for dynamic characteristics estimation of subsurface using microtremor on the ground surface. Quarterly report of Railway Technical Research Institute, 30(1), pp.25-33.

Nakamura, Y. (2008). On the H/V spectrum. Proceedings of the 14th World Conference on Earthquake Engineering, Beijing, China, 12-17 October 2008.

Nakamura, Y. (2010). Comment on "Microtremor measurements in the Nile delta basin, Egypt: Response of the topmost sedimentary layer" by E.A. Fergany and S. Bonnefoy-Claudet. Seismological Research Letters, v.81(2), pp.241-243.

Nakamura, T., S. Tsuboi, Y. Kaneda, Y. Yamanaka (2009). Rupture process of the 2008 Wenchuan, China earthquake inferred from teleseismic waveform inversion and forward modeling of broadband seismic waves. Tectonophysics, v.491(1-4), pp.72-84.

Nishimura, N., Yagi, Y. (2008). Rupture Process for May 12, 2008 Sichuan Earthquake (Ver. 2). http://www.geol.tsukuba.ac.jp/~nisimura/20080512. Last accessed May 2009.

Nyst, M., Thatcher, W. (2004). New constraints on the active tectonic deformation of the Aegean. Journal of Geophysical Research, v.109(B11), pp.406-430.

Olsen, K.B., Madariaga, R., Archuleta, R.J. (1997). Three-dimensional dynamic simulation of the 1992 Landers earthquake. Science, v.278, pp.834-838.

Ordóñez, G.A. (2011). SHAKE2000 A computer program for the 1-D analysis of geotechnical earthquake engineering problems. http://www.shake2000.com/. Last accessed April 2011.

Ottemöller, L., Voss, P., Havskov, J. (2011). SEISAN earthquake analysis software for Windows, Solaris, Linux and MacOSX, version 9.0, 2011.

Pankow, K.L., Pechmann, J.C. (2004). The SEA99 ground motion predictive relations for extensional tectonic regimes: Revisions and a new peak ground velocity relations. Bulletin of the Seismological Society of America, v.94(1), pp.341-348.

Papazachos, B., Papazachou, C. (1997). The earthquakes of Greece. Technical books Edition, Thessaloniki, 304p.

Papazachos, B.C., Papaioannou, C.A., Papazachos, C.B., Savvaidis, A.S. (1997). Atlas of isoseismal maps for strong shallow earthquakes in Greece and surrounding area (426BC-1995). Technical books Edition, Thessaloniki, 176p.

Peyrat, S., Olsen, K., Madariaga, R. (2001). Dynamic modeling of the 1995 Landers earthquake. Journal of Geophysical research, v.106(B11), pp.26,467-26,482.

Pitarka, A., Somerville, P., Fukushima, Y., Uetake, T., Irikura, K., (2000). Simulation of Near-Fault Strong-Ground Motion Using Hybrid Green's Functions. Bulletin of the Seismological Society of America, v.90(3), pp.566-586.

Pulido, N., Kubo, T. (2004). Near-fault strong motion complexity of the 2000 Tottori earthquake (Japan) from a broadband source asperity model. Tectonophysics, v.390(1-4), pp.177-192.

Pulido, N., Ojeda, A., Atakan, K., Kubo, T. (2004). Strong ground motion estimation in the Sea of Marmara region (Turkey) based on a scenario earthquake. Tectonophysics, v.391(1-4), pp.357-374.

Reiter, L. (1990). Earthquake Hazard Analysis: Issues and Insights. Columbia University Press, New York, 254p.

Smith, W.H.F., Wessel, P. (1990). Gridding with continous curvature splines in tension. Geophysics, v.55(3), pp.293-305.

Somerville, P., Sen, M., Cohee, B. (1991). Simulation of strong ground motions recorded during the 1985 Michoacán, Mexico and Valparaiso, Chile earthquakes. Bulletin of the Seismological Society of America, v.81, pp.1-27.

Spudich, P., Fletcher, J.B., Hellweg, M., Boatwright, J., Sullivan, C., Joyner, W.B., Hanks, T.C., Boore, D.M., McGarr, A., Baker, L.M., Lindh, A.G. (1997). SEA96 – A new predictive relation for earthquake ground motions in extensional tectonic regimes. Seismological Research Letters, v.68(1), pp.190-198.

Sørensen, M.B., Atakan, K., Pulido, N. (2007a). Simulated strong ground motions for the great M 9.3 Sumatra-Andaman earthquake of 26 December 2004. Bulletin of the Seismological Society of America, v.97(1A), pp.S139-151.

Sørensen, M.B., Pulido, N., Atakan, K. (2007b). Sensitivity of ground motion simulations to earthquake source parameters: a case study for Istanbul, Turkey. Bulletin of the Seismological Society of America, v.97(3), pp.881-900.

Taymaz, T., Yilmaz, Y., Dilek, Y., (2007). The geodynamics of the Aegean and Anatolia: Introduction. In: The geodynamics of the Aegean and Anatolia. Editors: Taymaz, T., Yilmaz, Y., Dilek, Y., Geological Society Special Publication, v.291, pp.1-16.

ten Veen, J.H. (2004). Extension of Hellenic forearc shear zones in SW Turkey: the Pliocene-Quaternary deformation of the Eşen Cay Basin. Journal of Geodynamics, v.37(2), pp.181-204.

Teves-Costa, P., Matias, L., Bard, Y.-B. (1996). Seismic behavior estimation of thin alluvium layers using microtremor recordings. Soil Dynamics and Earthquake Engineering, v.15(3), pp.201-209.

USGS (2009). Magnitude 7.9 – Eastern Sicuan, China. http://earthquake.usgs.gov/eqcenter/eqinthenews/2008/us2008ryan/#details. Last accessed July 2009.

USGS Landslide Hazard Program (2009). Landslides From the Sichuan (Wenchuan) Earthquake, China, May 2008. http://landslides.usgs.gov/learning/photos/international/landslides_from_the_sichuan_wenchuan_earthquake_china_may_2008. Last accessed September 2009.

Utheim, T., Havskov, J. (1998). The SEISLOG Data Acquisition System. PC version, Guide to installation, maintenance and daily operation of the system. Institute of Solid Earth Physics, University of Bergen, Norway.

Wathelet, M. (2010). Geopsy project. http://www.geopsy.org/index.html. Last accessed March 2011.

Wald, D.J., Quitoriano, V., Heaton, T.H., Kanamori, H. (1999). Relationships between peak ground acceleration, peak ground velocity and Modified Mercalli Intensity in California. Earthquake Spectra, v.15(3), pp.557-564.

Wang, W.M., Zhao, L.F., Li, J., Yao, Z.X. (2008). Rupture process of the Ms 8.0 Wenchuan earthquake of Sichuan, China (in Chinese). Journal of Geophysics, v.51(5), pp.1403-1410.

Wells, D.L., Coppersmith, K.J. (1994). New empirical relationships among magnitude, rupture length, rupture width, rupture area, and surface displacement. Bulletin of the Seismological Society of America, v.84(4), pp.974-1,002.

Wessel, P., Smith, W.H.F. (1998). New, improved version of Generic Mapping Tools released. EOS, Tansactions, American Geophysical Union, v.79(49), pp.579-579.

Yin, Y.P. (2008). Researches on the geo-hazards triggered by Wenchuan earthquake, Sichuan. Journal of Engineering Geology, v.16(4), pp.433-444, in Chinese.

Zhang, Y., Feng, W.P., Xu, L.S., Zhou, C.H., Chen, Y.T. (2008). Spatial-temporal rupture process of the 2008 Wenchuan earthquake. Science of China, v.38(10), pp.1,186-1,194.

Zhang, P., Yang, Z.X., Gupta, H.K., Bhatia, S.C., Shedlock, K.M. (1999). Global seismic hazard assessment program (GSHAP) in continental Asia. http://www.seismo.ethz.ch/GSHAP/eastasia. Last accessed April 2011.

Zhao, C.P., Chen, Z.L., Zhou, L.Q., Li, Z.X., Kang, Y. (2010). Rupture process of the Wenchuan M8.0 earthquake of Sichuan, China: the segmentation feature. Chinese Science Bulletin, v.55(3), pp.284-292.

Zhao, Z., Zhang, R. (1987). Preliminary study of crustal and upper mantle velocity structure of Sichuan Province (in Chinese). ACTA Seismologica Sinica, v.9, pp.99-106.

Zifa, W. (2008). A preliminary report on the Great Wenchuan Earthquake. Earthquake Engineering and Engineering Vibration, v.7(2), pp.225-234.